APPENDIX C4: Design of Sailplanes

This appendix is a part of the book **General Aviation Aircraft Design: Applied Methods and Procedures** by Snorri Gudmundsson, published by Elsevier, Inc. The book is available through various bookstores and online retailers, such as www.elsevier.com, www.amazon.com, and many others.

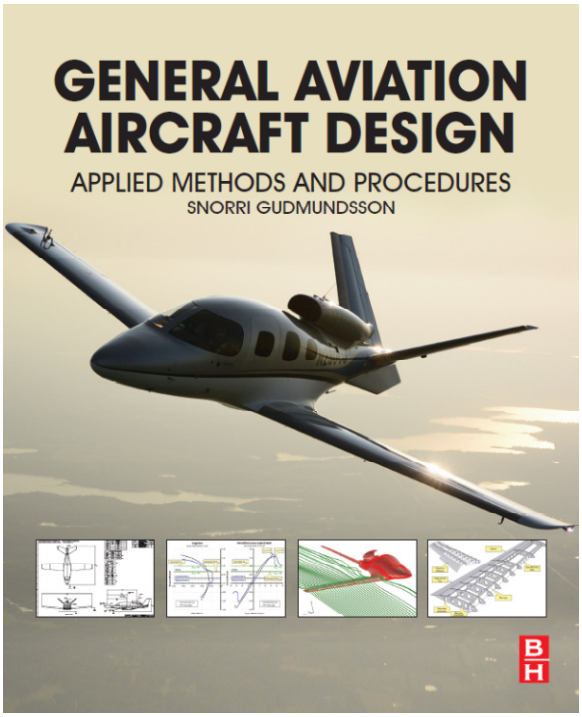

The purpose of the appendices denoted by C1 through C5 is to provide additional information on the design of selected aircraft configurations, beyond what is possible in the main part of Chapter 4, *Aircraft Conceptual Layout*. Some of the information is intended for the novice engineer, but other is advanced and well beyond what is possible to present in undergraduate design classes. This way, the appendices can serve as a refresher material for the experienced aircraft designer, while introducing new material to the student. Additionally, many helpful design philosophies are presented in the text. Since this appendix is offered online rather than in the actual book, it is possible to revise it regularly and both add to the information and new types of aircraft. The following appendices are offered:

C1 – Design of Conventional Aircraft
C2 – Design of Canard Aircraft
C3 – Design of Seaplanes
C4 – Design of Sailplanes (this appendix)
C5 – Design of Unusual Configurations

Figure C4-1: A Rolladen-Schneider LS-4 sailplane touching down using standard tail-first technique. Note the deployed spoilers on the upper surface of the wing. The sleekness of sailplanes would make them very hard to land were it not for spoilers that allow the drag to be increased temporarily during approach to landing, enabling standard approach angles to be used. (Photo by Phil Rademacher)

C4.1 Design of Sailplanes

Flying sailplanes and gliders remains a very popular past-time for many people. Gliding is the oldest form of heavier than air flight, dating back to the days of Otto Lilienthal (1848-1896) who pioneered the craft. For many, the absence of power offers incomparable simplicity and purity that allows the aviator to experience what it is to fly like the birds. However, the apparent simplicity is a veil that covers a level of design sophistication far superior to most GA aircraft. This appendix scratches the surface of conceptual design of sailplanes.

C4.1.1 Sailplane Fundamentals

Configuration A in Figure C4-2 presents an example of what the typical modern sailplane looks like. No aircraft generate less drag than sailplanes; their efficiency is a marvel of engineering. **Configuration B** is an example of a long endurance UAV, which "borrows" many sailplane features. The typical sailplane carries one to two people, it has a gross weight ranging from 800 to 1800 lb_f, wingspan from 35 to 101 ft, wing Aspect Ratio from 10 to 51, and wing loading from 5-12 lb_f/ft^2. At this time, the largest sailplane in the world is the German built Eta, with a wingspan of 101 ft, AR of 51, and wing loading of 10.44 lb_f/ft^2. It is thought to have a glide ratio around 70 – this means a glide path angle of 0.8° - or a still air glide range of 115 nm from an altitude of 10000 ft. Today, serious sailplanes are only fabricated using composite materials that yield the smoothest aerodynamic surfaces possible.

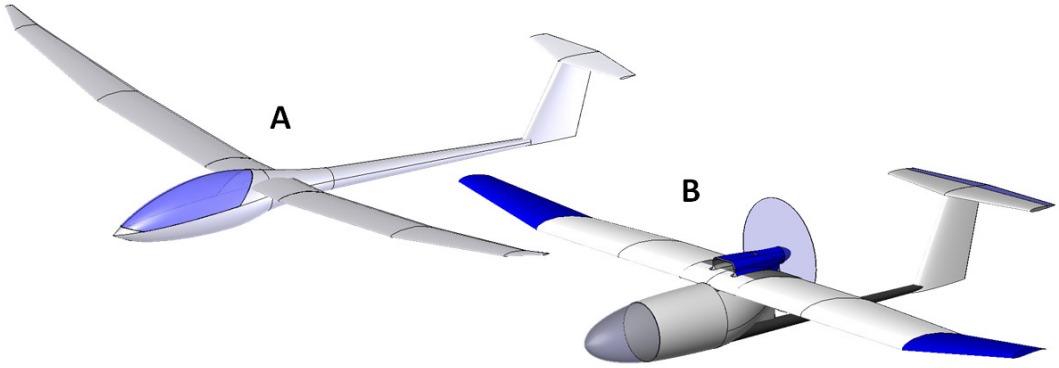

Figure C4-2: A sailplane (A) and a powered sailplane used as a UAV (B).

The modern sailplane features a tadpole fuselage, whose forward section is shaped to sustain laminar boundary layer naturally (Natural Laminar Flow or NLF) and contracted tail-boom to minimize the wetted area[1], once the boundary layer has transitioned into turbulent one. The fuselage is shaped to minimize the frontal area of the vehicle, but this requires the pilot to sit in an inclined position. More efficient sailplanes use a single piece canopy, which allows the NLF to extend farther aft on the fuselage than a two piece one. The modern sailplane uses a Schumann style wing planform (see Section 9.2.2, *The Schuemann Wing*) so its section lift distribution better resembles that of the harder to manufacture elliptical wing planform. Sometimes polyhedral dihedral is employed to reduce lift-induced drag further (see Section 10.5.9, *The Polyhedral Wing(tip)*). The most significant contributor to the low drag properties of sailplanes is its wing, and horizontal and vertical tails, all which feature NLF airfoils. Sailplanes usually utilize T-tails to place the HT outside of the turbulent wake of the fuselage. This helps sustaining a stable NLF over its surface. Section C4.1.4, *Sailplane Tail Design* presents a method to help with the sizing and positioning of the HT.

Operation of Sailplanes

Sailplanes demand a lot from their operators and proper flying techniques require extensive pilot training. Pilots must know how best to position the sailplane "on tow", how to develop "feel" when searching for lift, how to get the most out of thermals, and how best to manage approach and landing, considering the lack of power reduces the room for error[2]. This requires the pilot to spend long hours sharpening these skills, sitting inclined in a tiny cockpit. For this reason, the sailplane designer must be mindful of cockpit ergonomics, in addition to other factors (performance, stability, transportation, maintenance, etc.).

Sailplanes are designed to offer the largest glide ratio possible and, ideally, this should be attainable at high airspeed (something that requires an extensive drag bucket, cruise flaps, or jettisonable water ballast). Their exceedingly low rate of descent allows them to stay aloft for long periods, provided atmospheric convection is present. This is possible because even the most anemic atmospheric convection rises faster than the rate of descent for such vehicles.

Sailplane pilots take advantage of four kinds of convection (rising air); *thermals*, *ridge lift*, *standing mountain waves*, and *convergence lift*. Sailplane pilots refer to these as *lift*. A thermal is a column of rising air due to the ground being heated by the sun. The warmer air is less dense than the surrounding air, causing it to rise. Thermals can reach altitudes as high as 18000 ft, although 5000-6000 ft is more common. Thermals can often be identified by the cumulus clouds that reside on top of them. Ridge lift results from wind being forced over ground features, such as cliffs, mountains, and ridges. Wave lift is the consequence of oscillatory motion of air, referred to as gravity waves by atmospheric scientists. Sailplanes have reached altitudes in the upper 40000 ft while utilizing such lift. For instance, the cited altitude record below was achieved in such a wave. Convergence lift occurs when two masses of air collide, such as sea-breeze and inland air mass.

In addition to these, a gliding technique called *dynamic soaring* can be employed provided certain atmospheric conditions prevail. These are characterized by two air masses moving at different rates while being separated by a thin shear layer; a fictitious layer characterized by rapid change in wind speed. Such conditions typically exist near the ground between valleys of ocean waves or on the leeward side of ridges. The wind speed in the upper air mass is much greater when compared to the lower one and the two are separated by a steep speed gradient. The actual dynamic soaring consists of a set of maneuvers intended to systematically exchange kinetic and potential energy and make up for the energy lost to drag, by taking advantage of the gain in ground speed as the vehicle flies downwind (see Figure C4-3). This way, at **1**, the sailplane turns into the wind direction, still below the shear layer where the wind speed is negligible. At **2** it has begun a climb that will take it through the shear layer, where the headwind will now increase rapidly. The true airspeed and, thus, the dynamic pressure acting on the vehicle rise sharply as its inertia drives it through the oncoming wind flow. The rise of lift is instantly transformed into climb to a higher altitude. At the same time, its airspeed is reduced gradually. To prevent too much loss in airspeed, the vehicle banks sharply at **3** and begins a dive toward the ground with the wind becoming a tailwind. At **4**, the vehicle penetrates the shear layer again, now having accelerated with respect to the ground thanks to the tailwind. At **5**, the vehicle begins a new bank to change the heading into the wind and repeat the cycle.

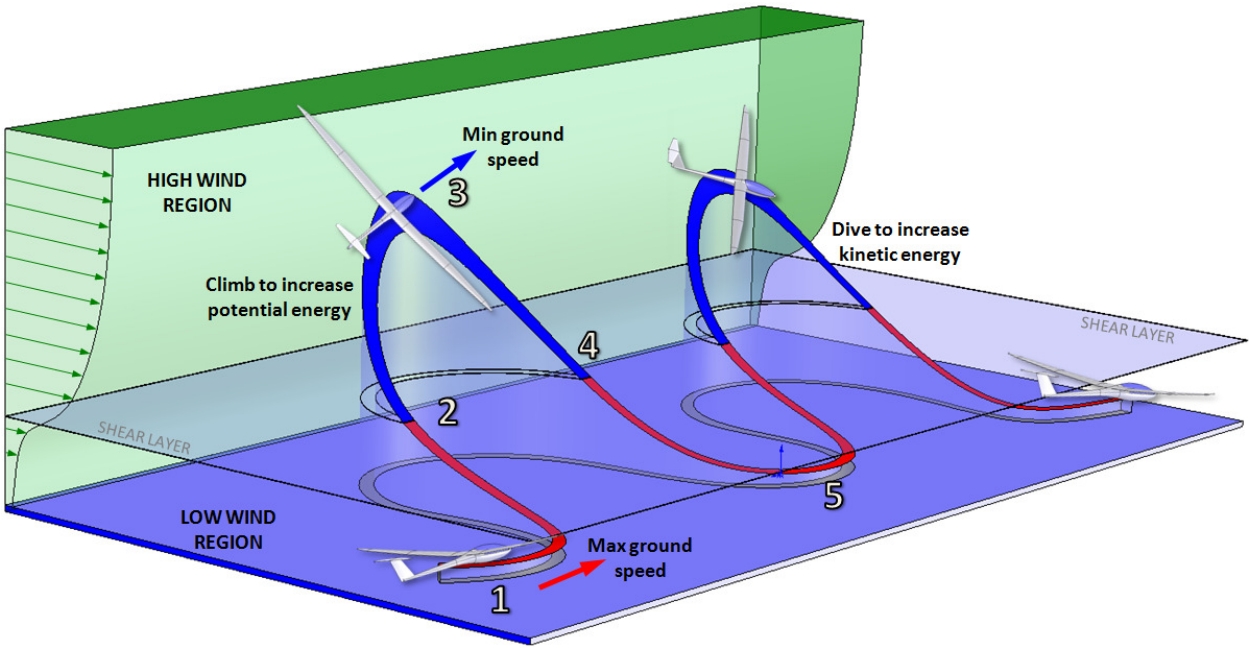

Figure C4-3: The basics of dynamic soaring.

Dynamic soaring is utilized by many species of seabirds, some which use it to travel great distances. However, no bird species rivals the Albatross, who regularly travel thousands of miles in a single trip, with minimal flapping of the wings, effectively gliding across oceans. Among humans, the method is used both among pilots of sailplanes and radio-controlled aircraft.

Long distance flying in sailplanes simply involves taking advantage of the energy available in the atmosphere that can be used to maintain necessary altitude. The pilot will ride the lift as high as possible before proceeding to the next source of rising air. As such, the typical cross-country sailplane flight consists of a climb, followed by a descent, followed by another climb, and so forth. It is possible to reach very high altitudes in the process. Altitudes exceeding 30000 ft is a common occurrence and certainly requires an oxygen bottle to be carried along. The current altitude record in a sailplane is 50722 ft (15460 m), set on 29th of August, 2006 by the Americans Steve Fossett (1944-2007) and Einar Enevoldson, in a modified Glaser-Dirks DG-505 Open Class sailplane[3]. The current long range record stands at about 1214 nm (2248 km), set by Klaus Ohlman on 2nd of December, 2003, on a Schempp-Hirth Nimbus Open Class sailplane[4].

Sailplane Airfoils

The modern sailplane uses sophisticated NLF airfoils, capable of sustaining laminar boundary layer up to 75% of the chord on the upper surface and 95% on the lower one. It is to be expected that such airfoils would yield lift and drag characteristics that are quite different from airfoils typically selected for powered airplanes. This leads to a new paradigm in sailplane design: Standard drag models are usually abandoned, as are conventional performance analysis methods that are associated with them. Instead, performance must be based on drag modeling that accurately accounts for the size of the drag bucket.

Many sailplanes feature "cruise" flaps, which is means to raise the normal flaps a few degrees Trailing Edge Up (TEU) above neutral deflection. This shifts the drag polar toward a lower C_L and, therefore, the L/D curve as well. Therefore, the maximum Lift-to-Drag (LD_{max}) is achievable at a higher airspeed, which is very beneficial in long distance competition. A typical drag polar and L/D graph for a modern sailplane airfoil is shown in Figure C4-4. The unconventional shape of the L/D curve is evident.

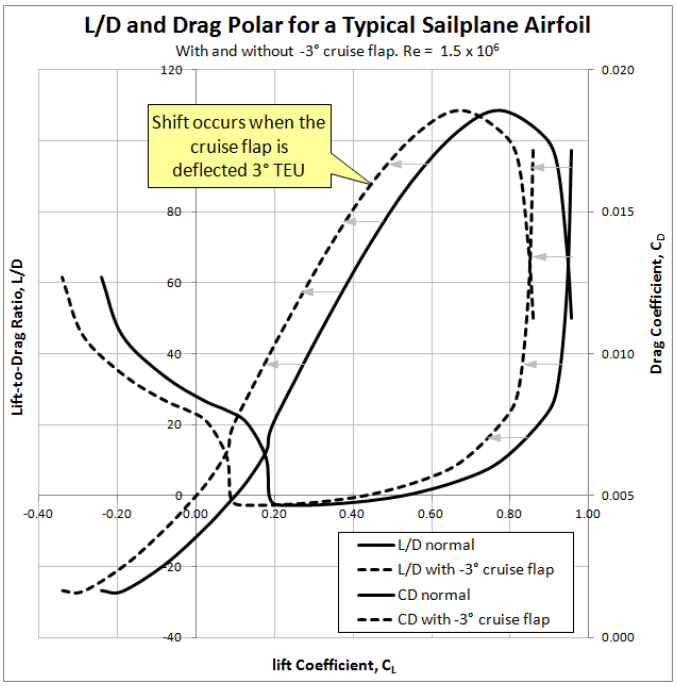

Figure C4-4: Lift and drag characteristics of a typical modern sailplane airfoil. The graph is based on experimental data from Reference 5.

Sailplanes generally operate at Reynolds Numbers that places their airfoils close to where the boundary layer is sensitive to transition from laminar to turbulent (see Figure C4-5); the *transition region*. It is bounded on the lower end by an expedited transition in high-turbulence environment (e.g. as encountered in wind tunnels) and the upper by what is possible in smooth atmosphere. To take advantage of the low drag associated with laminar boundary layer and to delay the transition of the boundary layer requires very smooth surfaces.

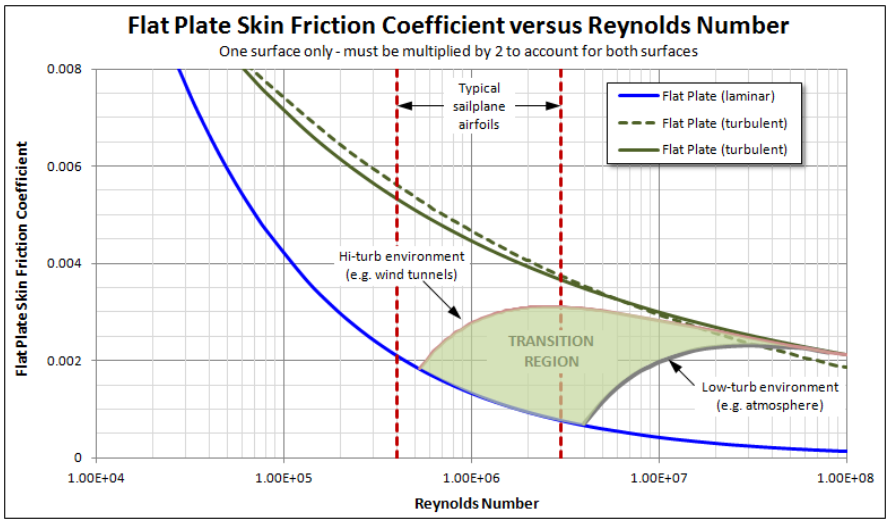

Figure C4-5: Sailplanes operate in the transition region and must feature smooth surfaces to delay transition from laminar to turbulent boundary layer. (Adapted from Reference 6)

The Importance of the Drag Bucket

Figure C4-6 is an idealized representation intended to show the importance of achieving NLF on a hypothetical sailplane. The shape of both the drag polar and L/D curve is classical for all NLF airfoils that feature a distinct two-wall drag bucket, including the double peak shape of the L/D curve. For instance, this characteristic is present in most NACA 65- and 66-series airfoils. The figure shows the impact this has on the glide performance of a hypothetical sailplane. Reducing the C_{Dmin} by 30 drag counts (e.g. from 0.013 to 0.010) increases the maximum L/D ratio by 4.2 units and shifts its location to a much lower C_L. Lower C_L means the LD_{max} will be realized at higher airspeed; something very beneficial to a sailplane (and would be to a powered cruiser as well). Admittedly 30 drag counts are on the high end of drag reduction and often the drag characteristics of the airplane as a whole mask the presence of the drag bucket, so a distinct double-peak LD curves is not always achieved for many applications. Instead, the laminar bucket shifts or widens the range of C_L, where "near" LD_{max} performance is found.

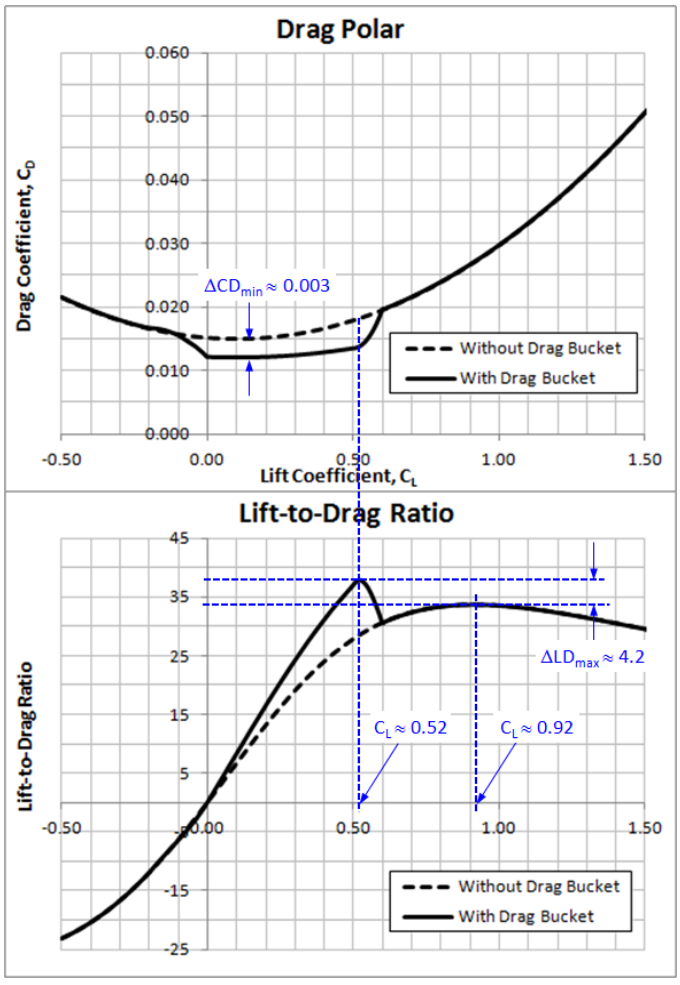

Figure C4-6: Example of the benefit of achieving NLF on a hypothetical sailplane.

As an example of the flexibility this yields, consider two sailplanes, A and B, which are identical except A does not develop a laminar drag bucket, while B does. Assume a wing loading of 10 lb_f/ft^2 and that they are subject to the glide characteristics presented in Figure C4-6 (i.e. turbulent and laminar drag). Now consider a T-O scenario in which the sailplanes are towed to an altitude of 1500 ft AGL on a calm, sunny day and set out to reach a thermal some 4 nm away. Naturally, if the thermal is absent, the pilots must return to base, which begs the question; is there enough altitude remaining for the return flight? Using the performance methods of Chapter 21, *Performance - Descent* and noting that maintaining the airspeed for LD_{max} minimizes altitude loss, it is easy to show that Sailplane A achieves its LD_{max} at 58 KTAS, while B achieves it at 77 KTAS. It will take Sailplane A about 4m09s to cover a distance of 4 nm, while B covers it in 3m07s. Sailplane A loses 719 ft of altitude in the process and, upon return will be about 62 ft above the ground, requiring perfect piloting for the entire duration of the flight. Sailplane B loses 640 ft of altitude and will have some 220 ft upon return. Naturally, things are more complicated than this, although, in effect, this makes the point that a capable sailplane needs more than just a high LD_{max}; it should also achieve it at the lowest C_L possible.

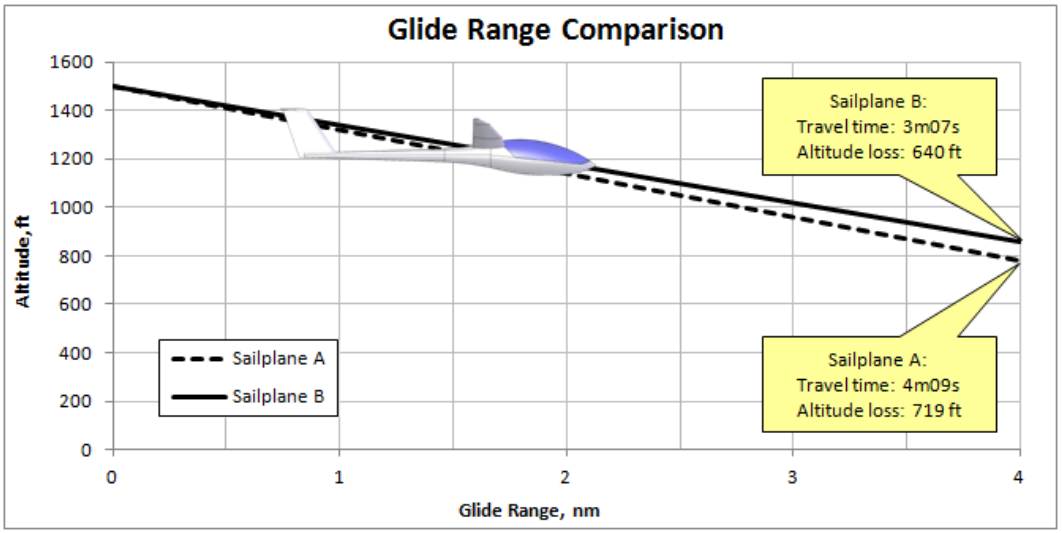

Figure C4-7: Glide range for two identical sailplanes. Sailplane A does not develop NLF, but B does.

Classes of Sailplanes

The mission definition of sailplanes depends on factors such as how and where it is going to be used. Is it intended for training, competition, aerobatics, and so on? And what is the nature of updrafts it should be designed to operate in; in other words, is it thermals or mountain waves? Sailplane design is also contingent upon the "class" it is slated for, as defined by the Fédération Aéronautique Internationale (FAI - The World Air Sports Federation) and listed in Table C4-1:

Table C4-1: Classes of Competition Sailplanes per FAI Definition.

Class Name	Description
Open Class	No restrictions. Max mass is 850 kg (1875 lb_f)
Standard Class	Max wingspan 15 m (49.2 ft), no camber changing devices, max mass is 525 kg (1159 lb_f)
15 meter Class	Max wingspan 15 m (49.2 ft), camber changing devices permitted, max mass is 525 kg (1159 lb_f)
18 meter Class	Max wingspan 18 m (59.1 ft), max mass is 600 kg (1325 lb_f)
20 meter Two-Seater Class	Max wingspan 20 m (65.6 ft), max mass is 750 kg (1656 lb_f)
World class	Limited class for a single type of sailplane – the PW-5
Club Class	For older and smaller gliders. Handicap system is used to level the playing field.

C4.1.2 Sailplane Glide Performance

Since the standard operation of sailplanes excludes the use of power (self-launching sailplanes glide with engine power off), their flight is far more influenced by the presence of rising and sinking air, as well as head- and tailwinds. A deep understanding of glide performance is imperative for sailplane pilots, in particular when attempting to maximize range. This section focuses on a few important elements of glide performance. It is largely based on references such as Reichmann[7], Welch and Irving[2], Thomas[6], Stewart[8], and Scull[9]. In order to help explain the fundamentals of glide performance, the properties of Sailplane A, discussed above, will be utilized in the following discussion. To keep things manageable, a simplified quadratic drag model is used, given by $C_D = 0.010 + 0.01498 \cdot C_L^2$. Also, time is represented using a format in which 6.25 minutes would be written as 6m15s.

Glide Range and Glide Endurance

The *glide range* is the horizontal distance a gliding aircraft covers between two given altitudes. The maximum range in still air is obtained by maintaining the airspeed for minimum glide angle (or best angle of descent), denoted by V_{BG}. The *glide endurance* is the time that takes a gliding aircraft to descent between two given altitudes. The maximum endurance in still air is obtained maintaining the airspeed for minimum rate of descent, denoted by V_{BA}. This is shown schematically in Figure C4-8.

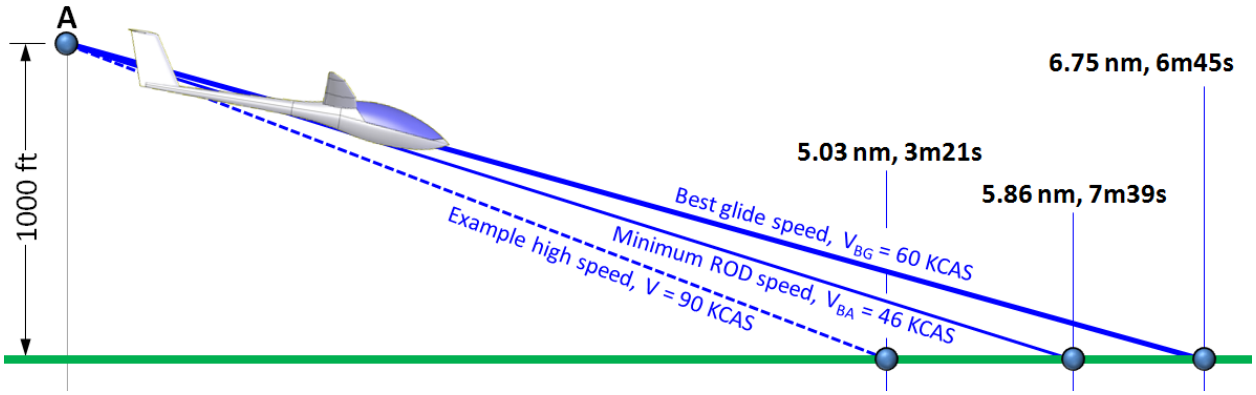

Figure C4-8: A simple schematic showing the impact of any particular airspeed on glide range and time aloft of Sailplane A, from an altitude of 1000 ft, assuming still air. In still air, V_{BG} always yields the longest range and V_{BA} the longest time aloft. Values are obtained using a flight polar like the one in Figure C4-9.

Basic Mathematical Relations for Glide Performance

The following expressions are derived in Chapter 21, *Performance – Descent* and are repeated here for convenience. All assume pure unpowered glide in still air and the simplified drag model.

Angle of descent:
$$\tan\theta = \frac{D}{L} = \frac{1}{L/D} \approx \frac{D}{W} \qquad (21\text{-}8)$$

Rate of descent:
$$V_V = \frac{DV}{W} = \frac{V}{(C_L/C_D)} \qquad (21\text{-}10)$$

Rate of descent:
$$V_V = \sqrt{\frac{2}{\rho\left(C_L^3/C_D^2\right)}\frac{W}{S}} = \frac{C_D}{C_L^{3/2}}\sqrt{\frac{2}{\rho}\frac{W}{S}} \qquad (21\text{-}12)$$

Sink rate while banking at ϕ:
$$V_V = \sqrt{\frac{2}{\rho\left((C_L\cos\phi)^3/C_D^2\right)}\frac{W}{S}} = \frac{C_D}{C_L^{3/2}\cos^{3/2}\phi}\sqrt{\frac{2}{\rho}\frac{W}{S}} \qquad (21\text{-}13)$$

Equilibrium glide speed

$$V = \sqrt{\frac{2\cos\theta}{\rho C_L}\frac{W}{S}} \qquad (21\text{-}11)$$

Airspeed of Minimum Sink Rate:

$$V_{BA} = \sqrt{\frac{2}{\rho}\left(\frac{W}{S}\right)}\sqrt{\frac{k}{3\cdot C_{D\min}}} \qquad (21\text{-}14)$$

Minimum Angle-of-Descent:

$$\tan\theta_{\min} = \frac{1}{LD_{\max}} = \sqrt{4\cdot k\cdot C_{D\min}} \qquad (21\text{-}15)$$

Best glide speed (still air):

$$V_{BG} = V_{LD\max} = \sqrt{\frac{2}{\rho}}\sqrt{\frac{k}{C_{D\min}}}\frac{W}{S} \qquad (21\text{-}16)$$

Glide range:

$$R_{glide} = h\cdot\left(\frac{L}{D}\right) = h\cdot\left(\frac{C_L}{C_D}\right) \qquad (21\text{-}17)$$

Where:

C_D = Drag coefficient
C_{Dmin} = Minimum drag coefficient
C_L = Lift coefficient
D = Drag
h = Altitude
k = Lift-induced drag constant
L = Lift
LD_{max} = Maximum lift-to-drag ratio
R_{glide} = Glide range
S = Reference wing area
V = Airspeed
V_{BA} = Airspeed of minimum rate of descent
V_{BG} = Airspeed of best glide (where LD_{max} occurs)
V_V = Vertical airspeed
W = Weight
ϕ = Bank angle
θ = Glide angle
θ_{min} = Minimum glide angle
ρ = Air density

The Basic Speed Polar – Optimum Glide in Still Air

Sailplane glide performance is determined using the *speed polar* (also called a flight polar); a diagram that shows the Rate-of-Descent (ROD) as a function of airspeed (for instance, see Section 21.3.2, *General Rate of Descent*). This is obtained by plotting the product –60·D·V/W versus airspeed.

Consider the basic speed polar of Figure C4-9, which shows the glide characteristics in still air and in the absence of lift or sink. Note that if the sailplane loses altitude, the value of the ROD is negative. A positive ROD means the sailplane is gaining altitude (climbing). Three important parameters are indicated; the stalling speed, V_S, the airspeeds of minimum ROD, V_{BA}, and minimum glide angle, V_{BG}. It can be seen that Sailplane A achieves a minimum ROD of 131 fpm at airspeed of 46 KCAS (V_{BA}) and LD_{max} of 40.9 is achieved at 60 KCAS (V_{BG}). The ROD at V_{BG} is 149 fpm. Maintaining V_{BA} will yield the longest time aloft (endurance), and V_{BG} yields the greatest distance flown (range). These are optimum values in no-wind, no-thermal conditions only.

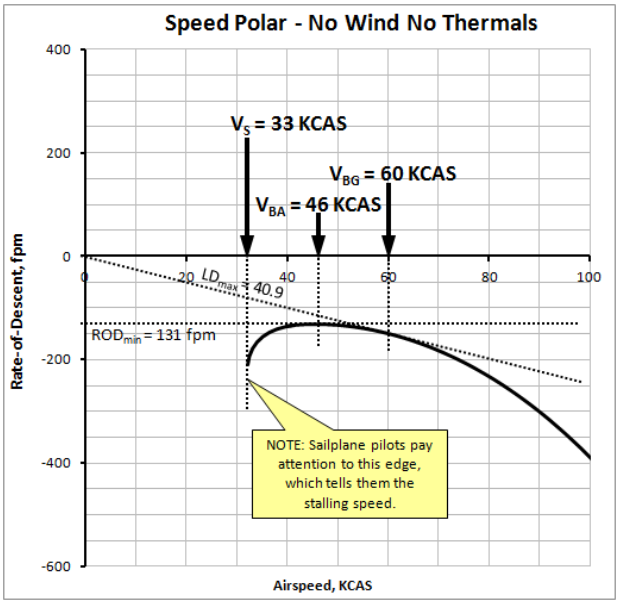

Figure C4-9: Basic speed polar for Sailplane A at S-L.

In the world of sailplane piloting, the stalling speed (V_S) is always indicated where the speed polar is terminated on the left hand side (see Figure C4-9). Note that the stalling speed shown leads to an unrealistically high C_{Lmax}, a fact we will conveniently ignore, as said sailplane is purely intended for explaining concepts.

It is important to keep the basic speed polar in mind when considering sailplanes subject to lift or sink and head- or tailwind.

The Speed Polar with Variable Wing Loading

The speed polar for the sailplane is often prepared with one or two specific and frequently used weights in mind. If the sailplane is loaded to higher weight, for instance, due to the addition of a second occupant or water ballast) the speed polar will be shifted to a higher airspeed when compared to the polar at a lighter weight (see Figure C4-10). The general rule-of-thumb is that there is no change in the LD_{max}, only in the airspeed at which it occurs. On the other hand, and as is to be expected, the magnitude of ROD_{min} increases, as does the airspeed at which it occurs. The figure shows this is akin to sliding the polar along the sloped line, although it also "expands" as shown.

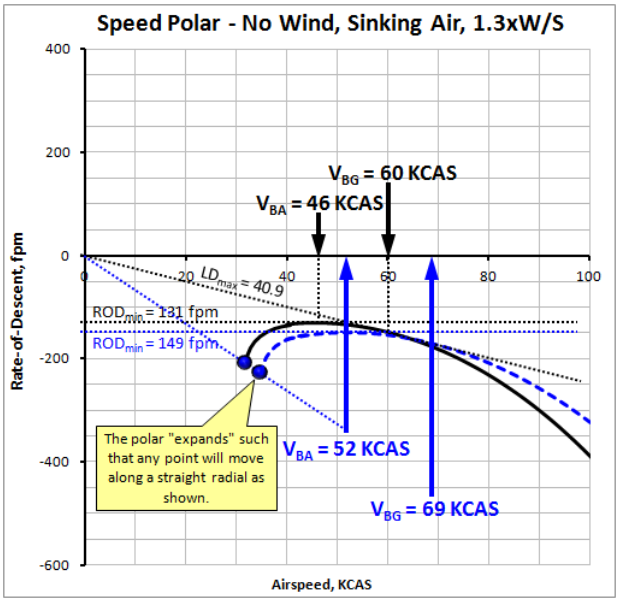

Figure C4-10: Basic speed polar for Sailplane A at S-L, while subject to 30% increase in weight.

In the case of Sailplane A, there is no change in the magnitude of the LD_{max}, but its airspeed increases from 60 to 69 KCAS with a 30% increase in weight. The magnitude of ROD_{min} increases from 131 to 149 fpm and its airspeed from 46 to 52 KCAS.

Optimum Glide in Sinking Air

If the sailplane enters a column of air sinking at some average rate, say 200 fpm (about 2 knots), this is akin to shifting the speed polar downward as shown in the left graph of Figure C4-11. It can be seen that this does not affect V_{BA}. However, V_{BG} is shifted to a higher airspeed, here, from 60 to 77 KCAS. As stated before, in the absence of lift or sink, the normal ROD at these two airspeeds is 131 (at V_{BA}) and 148 fpm (at V_{BG}), respectively. The effective LD_{max} (defined here as horizontal speed divided by the vertical speed) is reduced from 40.9 to 18.8. Note that it is not important whether the polar is shifted downward or the origin is shifted upward, as shown in the right graph of Figure C4-11. The right graph, thus, presents a clever method to determine the best airspeed-to-fly using a polar made for standard conditions only. This is discussed in more detail later.

To help understand why it is beneficial to increase the airspeed, assume the sailplane glides right through the center of a column of uniformly sinking air, whose diameter is 1 nm, and average rate is 200 fpm. At 60 KCAS, it will take the sailplane one minute flat to fly through the column, during which it is descends at 131 + 200 = 331 fpm. In other words, it loses 331 ft of altitude in the process. At 77 KCAS, the sailplane descends at 148 + 200 = 348 fpm and it will take 47 seconds to cruise through the column, during which it loses (47/60) x 348 = 273 ft. Therefore, less altitude is lost by flying at the higher airspeed. While the difference (58 ft) may seem trivial, it is of crucial importance to the precision piloting required to fly long distances competitively.

Figure C4-12 shows how the downdraft affects the glide from a different perspective; presenting it as L/D versus airspeed. The peak L/D is reduced and shifted to a higher airspeed.

Optimum Glide in Rising Air

If the sailplane enters a column of air rising at some average rate, say 200 fpm, this corresponds to shifting the speed polar upward by that amount, as shown in Figure C4-13. Again, this has no effect on V_{BA}, which now is analogous to V_Y (best Rate-of-Climb airspeed) for powered aircraft. Similarly, V_{BG} becomes the *best-angle-of-climb* airspeed (denoted by V_X for powered aircraft) and it should maintained in a straight and level flight inside a thermal to achieve the steepest climb angle (although flying in thermals usually requires circling flight, so this is not as simple as that). Note that shifting the polar downward or the origin upward yields the same answer (see Figure C4-11).

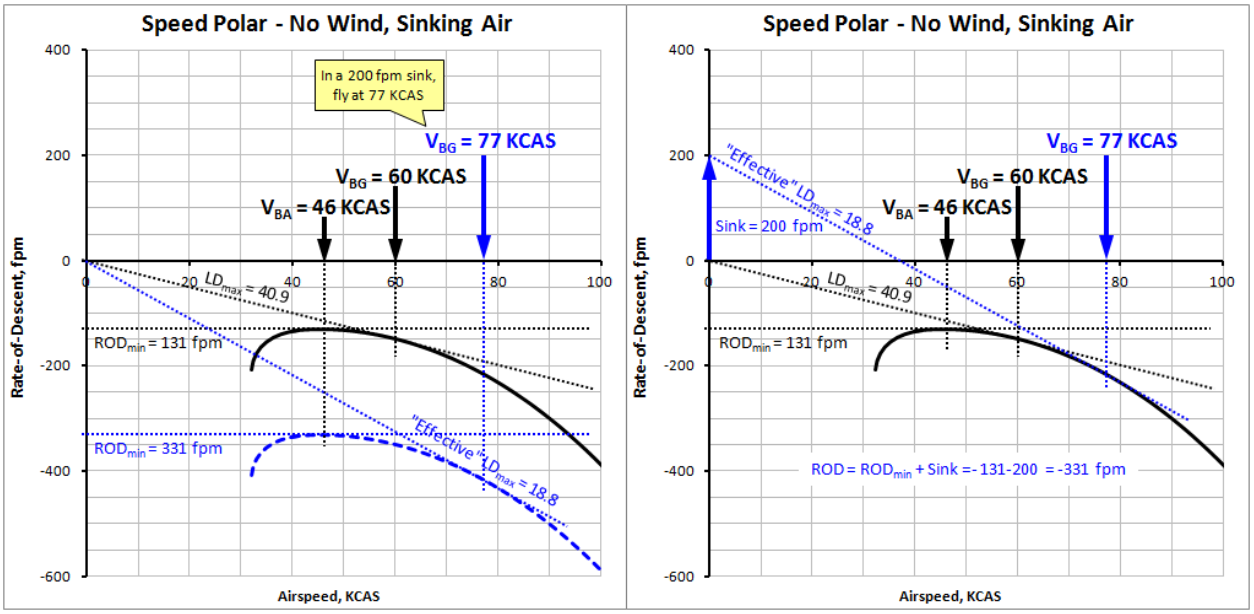

Figure C4-11: The speed polar for Sailplane A, assuming it enters a column of air sinking at 200 fpm (≈ 2 knots or 1 m/s). Both graphs display the same information. By shifting the origin of the vertical axis in the right graph up by 200 fpm, exactly the same answer is obtained as in the left graph.

Optimum Glide in Headwind or Tailwind

Consider Sailplane A gliding in a 10 knot headwind (or tailwind) while the pilot maintains a constant calibrated airspeed of 60 KCAS (i.e. by keeping the needle of the airspeed indicator pointing at 60 KCAS). With respect to the ground, the aforementioned glide speeds will occur 10 knots slower (or faster). This way, the normal best angle glide speed of 60 KCAS (V_{BG}) will actually correspond to 50 (or 70) KGS (Knots Ground Speed). If the pilot maintains 60 KCAS, the glide range of the sailplane (descending at 148 fpm) will vary greatly. The same holds for the glide angle, θ, with respect to the ground, which can be determined as follows:

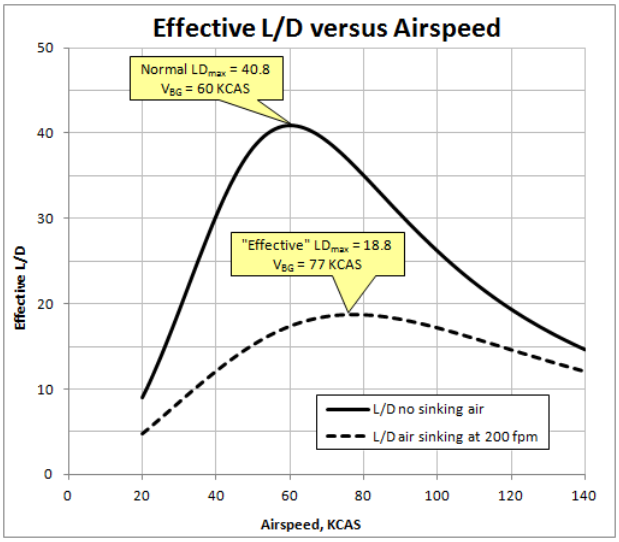

Figure C4-12: Standard and "effective" L/D curves for Sailplane A at S-L. The sink rate is 200 fpm.

In a 10 knot tailwind: $\theta = \tan^{-1}\left[(148/60)/(70\times1.688)\right] = 1.20°$ $\Delta\theta = -0.20°$

In no-wind conditions: $\theta = \tan^{-1}\left[(148/60)/(60\times1.688)\right] = 1.40°$

In a 10 knot headwind: $\theta = \tan^{-1}\left[(148/60)/(50\times1.688)\right] = 1.67°$ $\Delta\theta = +0.27°$

Where $\Delta\theta$ represents the difference between the still air and windy glide-angle condition. This is shown schematically in Figure C4-14. If the sailplane begins its glide 1000 ft above the ground, it will touch down in 1000/148 = 6m45s in all three cases, however, the range in headwind will be approximately (50 nm/60 min) x (6.75 min) = 5.63 nm, 6.76 nm in still air, and 7.88 nm in tailwind.

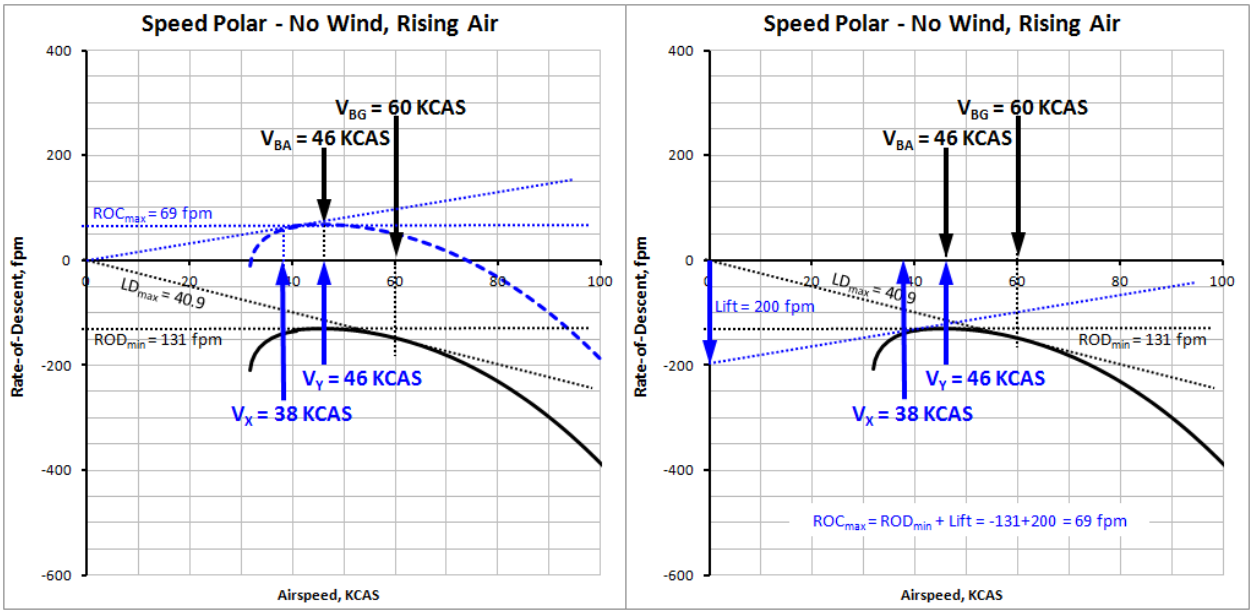

Figure C4-13: The speed polar for Sailplane A, assuming it enters a lift of 200 fpm (≈ 2 knots or 1 m/s). Both graphs display the same information. By shifting the origin of the vertical axis in the right graph down by 200 fpm, exactly the same answer is obtained as that in the left graph.

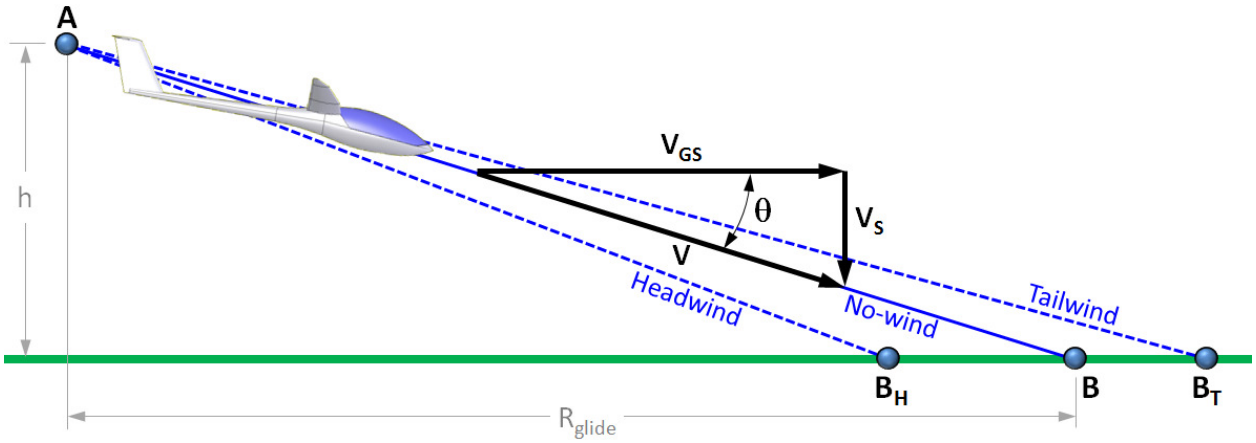

Figure C4-14: A simple schematic showing the impact of head- or tailwind on the glide range assuming the pilot maintains the same indicated (or calibrated) airspeed in all three cases.

This begs the question: In headwind, is there an airspeed other than 60 KCAS that yields range greater than 5.63 nm? To answer this question, assume that this time Sailplane A is being flown in a 10 knot headwind at 63 KCAS.

The ROD at this airspeed is 156 fpm. The ground speed will be 53 KGS and the glide will last for 1000/156 = 6m24s (approximately 6.40 min). In that time, it will cover (53 nm/60 min) x (6.40 min) = 5.65 nm, which is greater than 5.63 nm at 60 KCAS. This shows that increasing the airspeed (up to a certain point) in headwind, yields greater range. The inverse is true for tailwind.

It should be clear that a sailplane gliding in headwind equal to its forward speed in magnitude will not make any headway with respect to the ground. Rather it would descend vertically – its glide angle would be 90°. Horizontal distance can only be achieved by a forward glide speed faster than the headwind. The airspeed that yields the greatest range can be determined by shifting the origin of the speed polar horizontally by a distance that equals the wind speed, and then draw a tangent to the speed polar. Like the previous discussion demonstrates, in headwind, the origin of the coordinate system is shifted sideways to the right, while for tailwind it is shifted to the left, as shown in Figure C4-15.

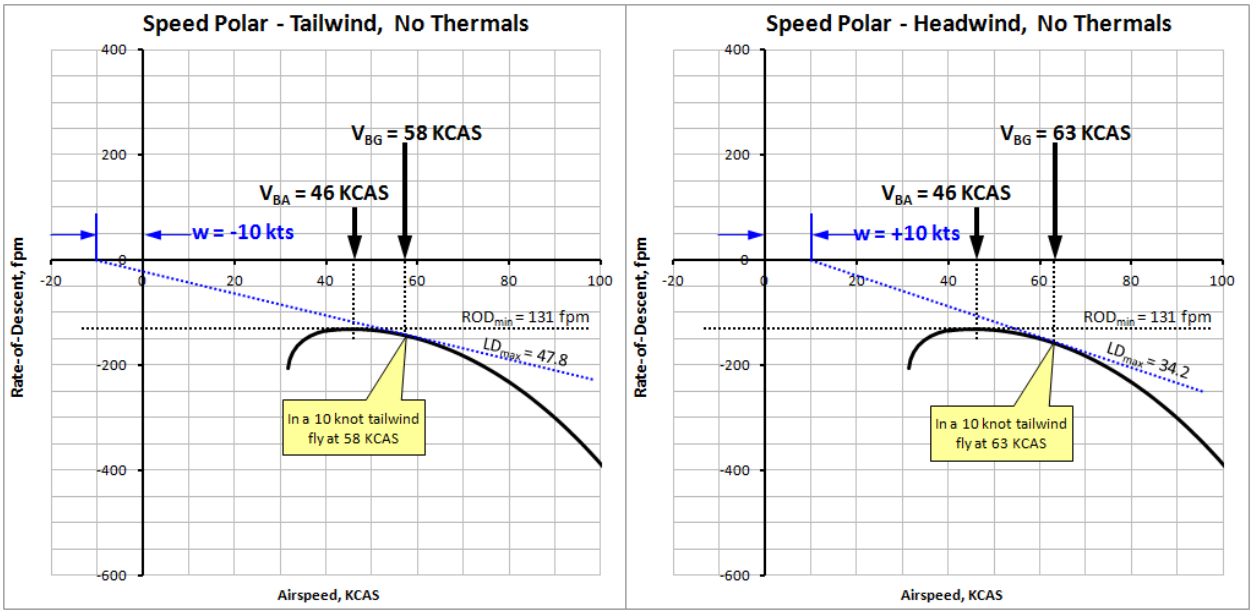

Figure C4-15: The speed polar for Sailplane A, for a glide in a 10 knot tail- and headwind. By shifting the origin of the horizontal axis to the left or right by 10 knots, an ideal airspeed for glide is obtained.

Speed-to-Fly

The preceding discussion shows that a speed polar for no wind, no thermal conditions can be used with ease to determine the proper airspeed to fly in any non-standard conditions in order to maximize the range of the sailplane. The particular airspeed obtained this way is referred to as *Speed-to-Fly* by sailplane pilots. It is determined by shifting the origin around as shown in Figure C4-17. For headwind, the origin is shifted to the right. For headwind and sink, it is shifted to the right and up, and so on.

Average Cross-Country Speed

Physics dictates that while cruising toward a thermal a sailplane will exchange altitude for distance. Ideally, once inside the thermal the altitude will eventually be recovered. The total time consumed to travel to the thermal and "get back" to the original altitude is a figure of merit not just for sailplanes, but also piloting skills in long distance competitions. Consider the sailplane depicted in Figure C4-16, where the segment A-B is the glide segment and B-C the climb segment. The *average cross-country speed*, denoted by V_{avg} (also shown in Figure C4-17) can be defined as the distance travelled to the thermal divided by the total time it takes to reach it and recover the lost altitude. Mathematically, this can be represented as follows:

$$V_{avg} = \frac{R_{glide}}{t} = \frac{R_{glide}}{t_{\text{glide}} + t_{\text{climb}}} \tag{C4-1}$$

Where t_{glide} and t_{climb} is the time spent in the glide and climb phases, respectively, and R_{glide} is the total distance covered. The three variables (R_{glide}, t_{glide}, and t_{climb}) are further defined as follows:

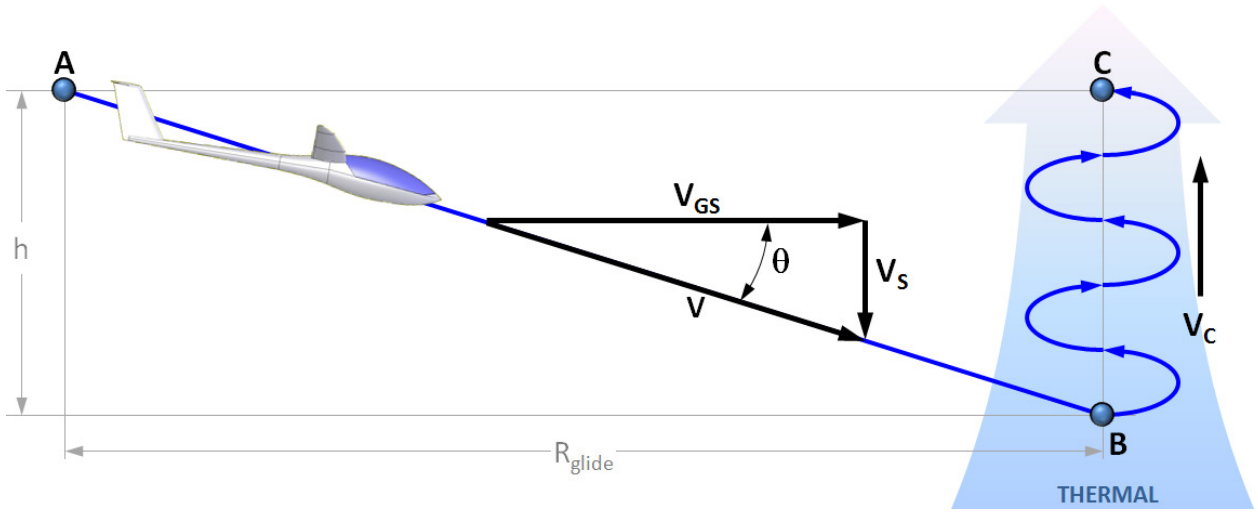

Figure C4-16: Definition of a *cross-country model*. (Adapted from Reference 6)

$$R_{glide} = \left(\frac{V_{GS}}{V_S}\right)H \qquad t_{\text{glide}} = \frac{H}{V_S} \qquad t_{\text{climb}} = \frac{H}{V_C} \tag{C4-2}$$

Where: V_S = Vertical speed in glide
V_{GS} = Arbitrary horizontal (forward) glide speed (see Figure C4-16)
V_C = Vertical speed in climb

Insert these into Equation (C4-1) and manipulate algebraically to yield:

$$V_{avg} = \frac{V_{GS}V_C}{V_C + V_S} \quad \Rightarrow \quad \frac{V_{avg}}{V_{GS}} = \frac{V_C}{V_C + V_S} \tag{C4-3}$$

The speed of climb, V_C, is the difference between the *thermal strength* (the rate at which air is rising), denoted by V_T, and the rate of sink of the sailplane as it circles inside the thermal, V_{SC}:

$$V_C = V_T - V_{SC} \quad \Rightarrow \quad \frac{V_{avg}}{V_{GS}} = \frac{V_T - V_{SC}}{V_T - V_{SC} + V_S} \tag{C4-4}$$

Optimum Speed-to-Fly between Thermals in Still Air

The preceding discussion pertains to the optimization of distance flown in still or moving air. It does not answer what optimum airspeed to maintain when flying between thermals and this must be answered for still or moving air as well.

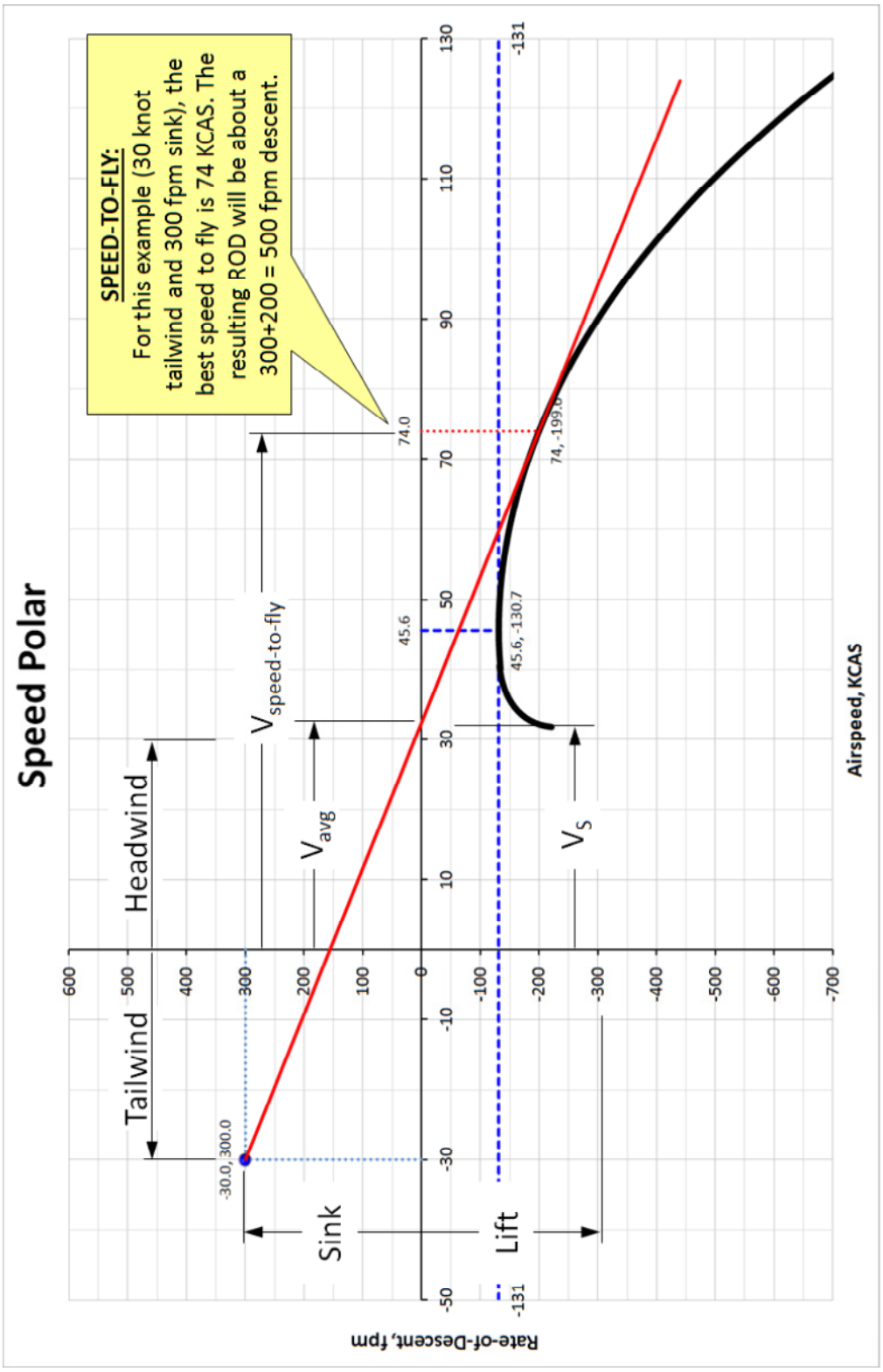

Figure C4-17: Putting it all together – here for Sailplane A. The appropriate directions in which to move the origin of the polar based on wind and thermal properties are shown. Then, a tangent from the offset origin to the polar is drawn to reveal the *Speed-to-Fly* and *average cross-country speed*.

Consider Sailplane A in Figure C4-18 at Point A, as it begins its 4 nm journey toward a thermal, some 2000 ft above the ground. Further, assume the thermal strength is known to be 400 fpm. Say the pilot considers 3 airspeeds to fly; $V_1 = V_{BG} = 60$ KCAS, $V_2 = 80$ KCAS, and $V_3 = 100$ KCAS. Each will lead to different results. Clearly, maintaining V_{BG}

will lead to the longest travel time (since it is the slowest speed), however, it also leads to the least amount of altitude to be made up. Conversely, maintaining V_3 leads to the earliest arrival time, but the greatest altitude to be made up. Details of this speed selection is shown in Table C4-2, which assumes uniform S-L atmospheric properties and that V_{BA} is maintained in the thermal in all three cases (in straight and level flight). It can be seen that the second airspeed, V_2 = 80 KCAS, is superior to the other two, as it leads to the least amount of total time required to reach the original altitude of 2000 ft. Consequently, its V_{avg} is the fastest.

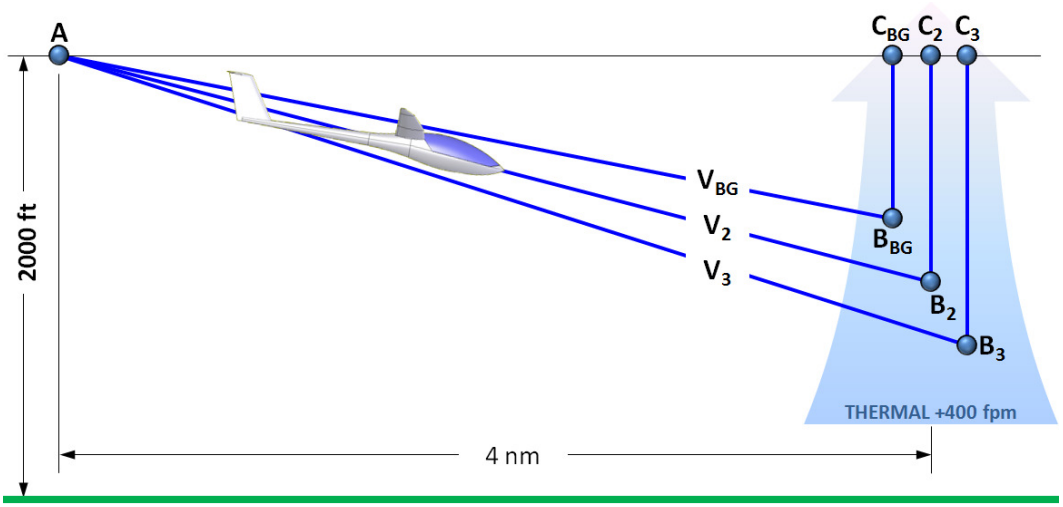

Figure C4-18: Sailplane A headed to a thermal whose strength is known to be 400 fpm.

Table C4-2: Summary of Trip Parameters for a 4 nm Cruise to a Thermal and Subsequent Climb to 2000 ft

Route	V	L/D	V_S, fpm		ΔH_{cruise}	Δt_{cruise}	Δt_{climb}	Δt_{total}	V_{avg}
	KCAS		in cruise	in thermal	ft	min	min	min	KCAS
A-B_{BG}-C_{BG}	60	40.9	-148	269	595	4.00	2.21	6.21	38.7
A-B_2-C_2	80	35.1	-230	269	693	3.00	2.57	5.57	43.1
A-B_3-C_3	100	26.2	-386	269	928	2.40	3.45	5.85	41.1

In addition to the airspeed, V, Table C4-2 shows the lift-to-drag ratio, vertical speed, V_S, in fpm, altitude lost en route, ΔH_{cruise}, in ft, time in cruise, Δt_{cruise}, time to climb back to 2000 ft, Δt_{climb}, and total time, Δt_{total}, all in minutes. The last column is an indication of progress made during the glide and subsequent climb. It is the average cross-country speed, here 4 nm divided by the total time, Δt_{total}.

Figure C4-19 shows how V_{avg} varies with $V_{speed\text{-}to\text{-}fly}$ for Sailplane A on an idealized no-wind day with a thermal of strength 400 fpm. It is assumed that the pilot maintains V_{BA} once entering the thermal and that the thermal is large enough to allow shallow bank angle to be maintained. The right graph shows how the speed polar can be used to extract $V_{speed\text{-}to\text{-}fly}$, while allowing V_{avg} to be extracted at the same time. Shift the origin to 269 fpm, which is the thermal strength (400 fpm) added to the ROD at V_{BA} (-131 fpm) to read 82 and 43 KCAS to be read, respectively. The mathematical derivation of why this leads to the correct result is beyond the scope of this text, but an interested reader is directed to Reference 7.

Optimum Speed-to-Fly between Thermals in Moving Air

If the sailplane is subject to lift or sink, as well as head- or tailwind, the V_{avg} and $V_{speed\text{-}to\text{-}fly}$ can be determined by moving the origin of the flight polar to a new position dictated by the wind and the expected climb rate in the thermal as explained earlier and as shown in the right graph of Figure C4-19. This airspeed can also be determined analytically using Equation (C4-3), which leads to the following solution that requires an iterative scheme to solve for the optimum lift coefficient, C_{Lopt}, given some expected rate-of-climb, V_C:

Optimum lift coefficient:

$$C_{D\min} - kC_{Lopt}^2 - V_C\sqrt{\frac{\rho S}{8W}}C_{Lopt}^{3/2} = 0 \qquad \text{(C4-5)}$$

With C_{Lopt} known, the average cross-country speed can be calculated from Equation (C4-6) below. Since the expression is actually applicable to any lift coefficient, C_L, this is used rather than C_{Lopt} to indicate this flexibility.

Average cross-country speed:

$$V_{avg} = \frac{V_C C_L^{-1/2}}{V_C\sqrt{\frac{\rho S}{2W}} + \frac{C_{D\min} + kC_L^2}{C_L^{3/2}}} \qquad \text{(C4-6)}$$

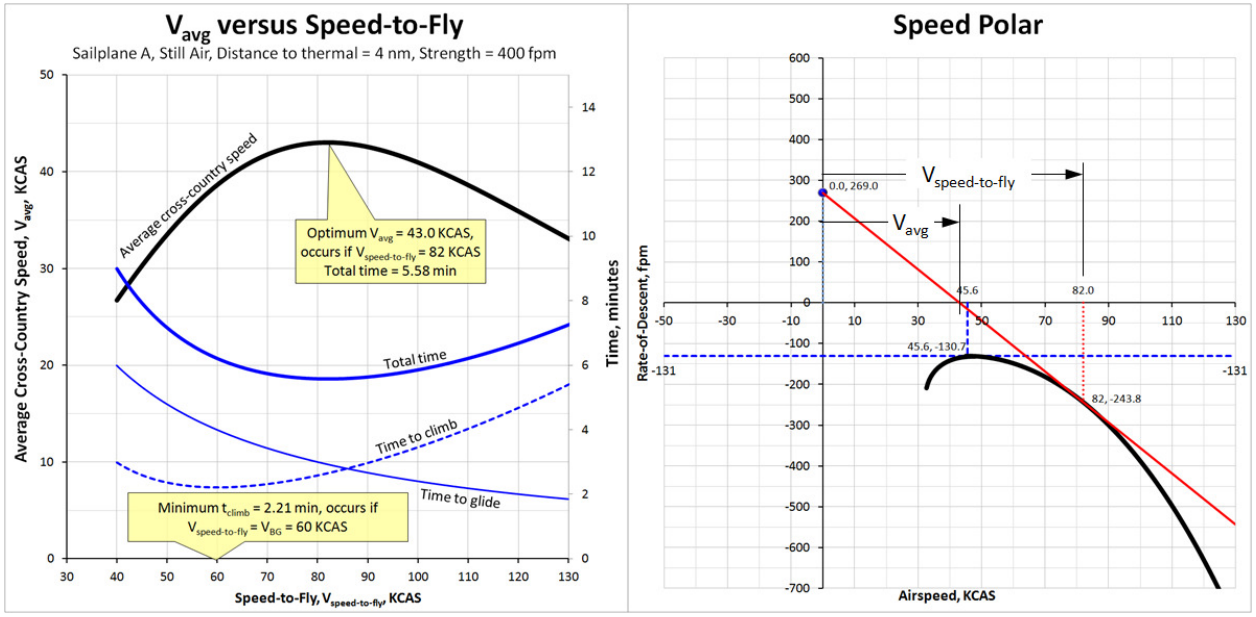

Figure C4-19: Left graph shows how V_{avg} varies with the Speed-to-Fly for Sailplane A under specific conditions. The right graph shows how the speed polar can be used to extract $V_{speed\text{-}to\text{-}fly}$ and V_{avg}.

DERIVATION OF EQUATIONS (C4-5) AND (C4-6):

The glide speed for a glide angle close to zero is given by Equation (21-11). Using small angle relations this is:

$$V_{GS} = \sqrt{\frac{2\cos\theta}{\rho C_L}\frac{W}{S}} \approx \sqrt{\frac{2}{\rho C_L}\frac{W}{S}}$$

The rate of descent is give by Equation (21-12): $V_V = V_S = \frac{C_D}{C_L^{3/2}}\sqrt{\frac{2}{\rho}\frac{W}{S}}$

Replacing the corresponding terms in Equation (C4-3) leads to:

$$V_{avg} = \frac{V_{GS}V_C}{V_C + V_S} = \frac{V_C\sqrt{\frac{2}{\rho C_L}\frac{W}{S}}}{V_C + \frac{C_D}{C_L^{3/2}}\sqrt{\frac{2}{\rho}\frac{W}{S}}} = \frac{V_C C_L^{3/2} C_L^{-1/2}\sqrt{\frac{2}{\rho}\frac{W}{S}}}{C_L^{3/2}V_C + C_D\sqrt{\frac{2}{\rho}\frac{W}{S}}} = \frac{V_C C_L^{-1/2}}{\frac{V_C}{\sqrt{\frac{2}{\rho}\frac{W}{S}}} + \frac{C_D}{C_L^{3/2}}} = \frac{V_C C_L^{-1/2}}{V_C\sqrt{\frac{\rho S}{2W}} + \frac{C_D}{C_L^{3/2}}}$$

If the drag is represented using the simplified drag polar, $C_D = C_{Dmin} + k\cdot C_L^2$, this becomes:

$$V_{avg} = \frac{V_C C_L^{-1/2}}{V_C\sqrt{\frac{\rho S}{2W}} + \frac{C_{D\min} + kC_L^2}{C_L^{3/2}}} = \frac{V_C C_L^{-1/2}}{V_C\sqrt{\frac{\rho S}{2W}} + \frac{C_{D\min}}{C_L^{3/2}} + kC_L^{1/2}} \qquad \text{(i)}$$

This is Equation (C4-6). The optimum C_L is obtained by differentiating Equation (i) with respect to C_L and setting the derivative to zero. Using the quotient rule of calculus (e.g. Section E.6.3, *Derivatives of Simple Functions*) where we define the functions f and g and their derivatives as follows:

$$f = V_C C_L^{-1/2} \quad \Rightarrow \quad df = -\frac{V_C C_L^{-3/2}}{2}$$

$$g = V_C\sqrt{\frac{\rho S}{2W}} + \frac{C_{D\min}}{C_L^{3/2}} + kC_L^{1/2} \quad \Rightarrow \quad dg = -\frac{3}{2}C_{D\min}C_L^{-5/2} + \frac{1}{2}kC_L^{-1/2}$$

Using this with the derivative of the function f/g (as stipulated by the quotient rule) we get:

$$\frac{dV_{avg}}{dC_L} = \frac{\left(-\frac{V_C C_L^{-3/2}}{2}\right)\left(V_C\sqrt{\frac{\rho S}{2W}} + \frac{C_{D\min}}{C_L^{3/2}} + kC_L^{1/2}\right) - \left(V_C C_L^{-1/2}\right)\left(-\frac{3}{2}C_{D\min}C_L^{-5/2} + \frac{1}{2}kC_L^{-1/2}\right)}{\left(V_C\sqrt{\frac{\rho S}{2W}} + \frac{C_{D\min}}{C_L^{3/2}} + kC_L^{1/2}\right)^2} = 0$$

Or more conveniently:

$$\left(-\frac{V_C C_L^{-3/2}}{2}\right)\left(V_C\sqrt{\frac{\rho S}{2W}} + \frac{C_{D\min}}{C_L^{3/2}} + kC_L^{1/2}\right) - \left(V_C C_L^{-1/2}\right)\left(-\frac{3}{2}C_{D\min}C_L^{-5/2} + \frac{1}{2}kC_L^{-1/2}\right) = 0$$

Some algebraic acrobatics of this equation leads to Equation (C4-5).

QED

The MacCready Speed Ring

Being able to accurately maintain the proper airspeed in a sailplane is vital for anyone striving to maximize the range. A selection of the optimized airspeed requires constant pilot awareness of the lift, sink, and wind speed in the immediate surroundings. For this reason, while flying long distances, the sailplane pilot may frequently adjust the airspeed to the variability of the atmosphere. To help, a special device called the *MacCready ring* is mounted to the variometer (the Rate-of-Climb indicator) in the sailplane. Essentially, the device is a dial or a ring, on which airspeeds for various sink or lift conditions are marked. The ring is rotated such that its index arrow indicates the lift expected in the next thermal. This rotates the airspeed markings such the needle of the variometer points at $V_{speed\text{-}to\text{-}fly}$, allowing the pilot to quickly read this airspeed without having to resort to the speed polar. The name of

the device is attributed to the late Dr. Paul MacCready (1925-2007) who developed it. More details on the operation of this device is beyond the scope of this text, but interested reader is pointed to any of the cited references and many other sources available and intended for sailplane pilots. Today, sailplanes use electronic variometers and flight computers that provide this information in real time.

Circling Flight

Once in a thermal, standard procedures call for the pilot to fly the sailplane in circles to take advantage of the rising air. Unfortunately, as the sailplane banks its sink rate (V_{SC}) increases over its value in straight and level flight (V_S). The steeper the bank, the greater is the sink rate and less potential energy is gained per unit time. The advantage of a steep bank is smaller turning radius, which allows the pilot to better maneuver inside the thermal and stay closer to its core region where lift is the greatest. This implies that an optimum bank angle exists that maximizes the rate of climb, given a specific turning radius and strength of lift.

Before determining this optimum bank angle, we must develop formulation that allows the sink rate to be assessed based on bank angle and turning radius. For this, consider Figure C4-20, which shows the forces acting on the sailplane banking at an angle ϕ, while flying at airspeed V. L is the lift, W the weight, m the mass, and R is the turn radius. If these are known, the sinking speed in circling flight can be determined from:

$$V_{SC} = \frac{C_D}{C_L^{3/2}} \sqrt{\frac{2}{\rho}\left(\frac{W}{S}\right)} \frac{1}{\left[1 - \left(\frac{2}{\rho}\left(\frac{W}{S}\right)\frac{1}{R \cdot g \cdot C_L}\right)^2\right]^{3/4}} \qquad \text{(C4-7)}$$

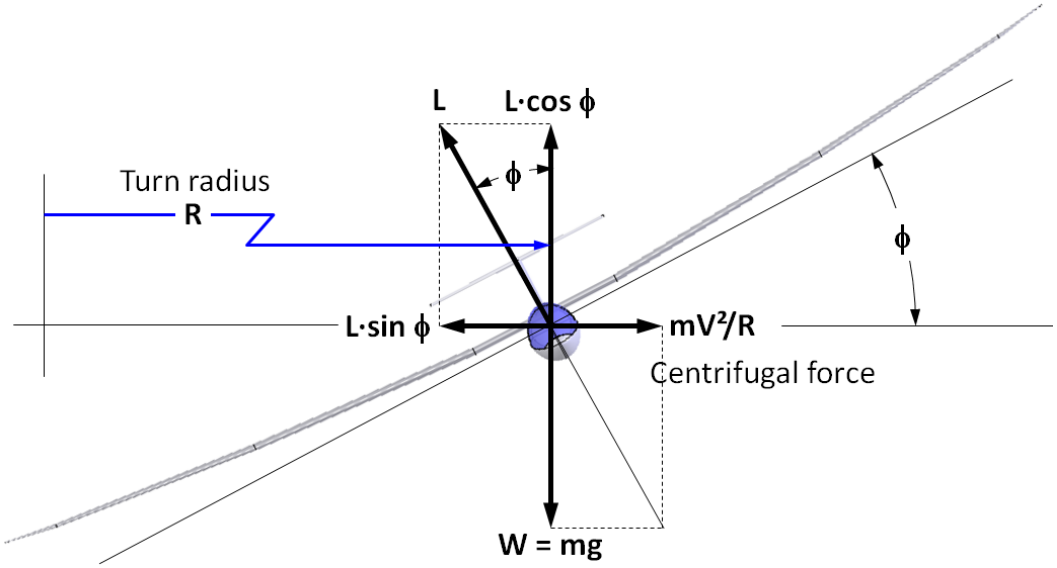

Figure C4-20: Forces acting on the sailplane as it is banked in a circling flight.

Using Equation (C4-7) the map shown in Figure C4-21 can be utilized to evaluate the turning performance of the sailplane, which is imperative for circling flight inside thermals. The diagram shows that if a given bank angle is maintained, the turn radius reduces only if the sailplane slows down. Similarly, for a fixed airspeed, the turn radius can only be reduced by banking steeper – which increases the sink rate further. It also shows that, for instance, for a 60° bank angle, the least sink rate is to be had around 67 KCAS, resulting in a turning radius of about 225 ft. Both styles of curves are plotted using Equation (C4-7). The solid curves are generated by first calculating C_L for a range of airspeeds using Equation (19-42) assuming a fixed ϕ. The C_Ls are then used to calculate C_D using the drag polar. The turning radius is also computed using Equation (iii) in the following derivation. Finally, these are inserted into

Equation (C4-7). The dashed curves are calculated for a range of turning radii and fixed airspeeds. First, the bank angle is calculated using Equation (i) in the derivation below. Then, this is used to calculate C_L and C_D as before. Again, these are inserted into Equation (C4-7).

Note that Equation (C4-7) can be used during the design stage to help shape parameters, such as wing area, AR, and drag characteristics, in an attempt to contour the turn performance curves towards a desirable turn radius and bank angle inside a thermal of specific characteristics. Of course, this must take into account the net rate of climb, $V_T + V_{SC}$, assuming V_{SC} has a negative value. Recall that V_T is the thermal strength (e.g. in ft/s or m/s) and V_{SC} is the rate of sink of the sailplane as it circles inside the thermal. A proper determination requires thermals to be modeled mathematically, as presented below.

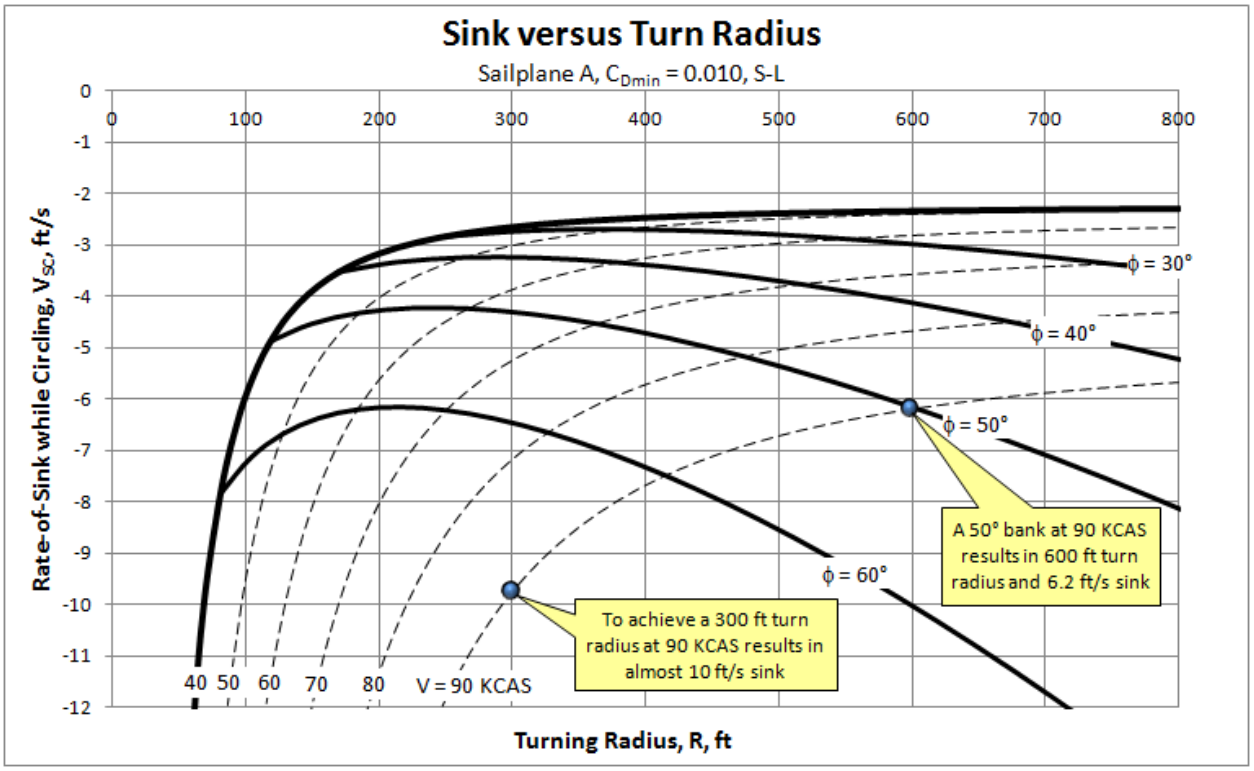

Figure C4-21: Turn performance map for Sailplane A, shows its rate-of-descent while banking at the specific angles and airspeeds.

DERIVATION OF EQUATION (C4-7):

The freebody diagram of Figure C4-20 shows that:

$$\tan\phi = \frac{mV^2/R}{mg} = \frac{V^2}{Rg} \qquad \text{(i)}$$

Therefore:

$$V = \sqrt{Rg\tan\phi} \qquad \text{(ii)}$$

or

$$R = \frac{V^2}{g\tan\phi} \qquad \text{(iii)}$$

Using these equations, any of the variables V, ϕ, and R, can be estimated if two of the others are known. Then, Equation (19-42), repeated here for convenience, can be used to estimate the speed of the airplane as a function of the lift coefficient, C_L, and bank angle, ϕ:

$$V = \sqrt{\frac{2W}{\rho S C_L}\left(\frac{1}{\cos\phi}\right)} \qquad (19\text{-}42)$$

More conveniently, the equation can be used to extract the lift coefficient, C_L, required during bank at a given airspeed, from which the drag coefficient, C_D, can be determined. Using Equation (ii) a relationship between the airspeed, bank angle, and turning radius can be established:

$$V^2 = \frac{2W}{\rho S C_L}\left(\frac{1}{\cos\phi}\right) = Rg\tan\phi = Rg\frac{\sin\phi}{\cos\phi}$$

Which leads to:

$$\sin\phi = \frac{2W}{\rho S C_L R g}$$

Using the trigonometric identity $\cos^2 x + \sin^2 x = 1$, it is now possible to write:

$$\cos\phi = \sqrt{1 - \left(\frac{2W}{\rho S C_L R g}\right)^2}$$

This relates the turning radius to the bank angle. Inserting this into Equation (21-13) yields Equation (C4-7).

QED

EXAMPLE C4-1:
Estimate the sink rate for Sailplane A as it banks 45° at an airspeed of 90 KCAS. Its wing loading is W/S = 10 lbf/ft². Use the drag model given earlier, $C_D = 0.010 + 0.01498 \cdot C_L^2$ and assume S-L conditions.

SOLUTION:
First estimate the lift coefficient at the condition using Equation (19-42):

$$C_L = \frac{2}{\rho V^2}\left(\frac{W}{S}\right)\left(\frac{1}{\cos\phi}\right) = \frac{2}{(0.002378)(90\times 1.688)^2}(10)\left(\frac{1}{\cos 45°}\right) = 0.5154$$

This contrasts 0.3644 for the straight and level condition at the same airspeed. Next calculate the drag coefficient:

$$C_D = 0.010 + 0.01498 C_L^2 = 0.010 + 0.01498(0.5154)^2 = 0.01398$$

Calculate the turn radius:

$$R = \frac{V^2}{g\tan\phi} = \frac{(90\times 1.688)^2}{(32.174)\tan 45} = 711 \text{ ft}$$

Then insert values into Equation (C4-7) to get the ROD in ft/s:

$$V_{SC} = \frac{C_D}{C_L^{3/2}}\sqrt{\frac{2}{\rho}\left(\frac{W}{S}\right)}\frac{1}{\left[1-\left(\frac{2}{\rho}\left(\frac{W}{S}\right)\frac{1}{R\cdot g\cdot C_L}\right)^2\right]^{3/4}}$$

$$= \frac{0.01398}{(0.5154)^{3/2}}\sqrt{\frac{2}{0.002378}(10)}\frac{1}{\left[1-\left(\frac{2}{0.002378}(10)\frac{1}{711\times 32.174\times 0.5154}\right)^2\right]^{3/4}} = 5.906 \text{ ft/s}$$

Thermal Velocity Profiles

The 3-dimensional shape of thermals is of vital importance to the design and operation of sailplanes. Since thermals are of finite dimension, the sailplane pilot must assertively bank inside it and ideally circle around its core while gaining as much altitude as possible. A small turning radius allows the maximum lift to be extracted out of the thermal. However, the smaller the turning radius the steeper is the bank required. This inevitably comes at the cost of reduced climb rate. Too shallow a bank will fly the sailplane out of the thermal. Too steep a bank will reduce the altitude gain and may even result in altitude being lost. Being able to mathematically describe the vertical velocity inside the thermal is thus fundamental to determine the optimum bank angle, given the distance of the sailplane from the core.

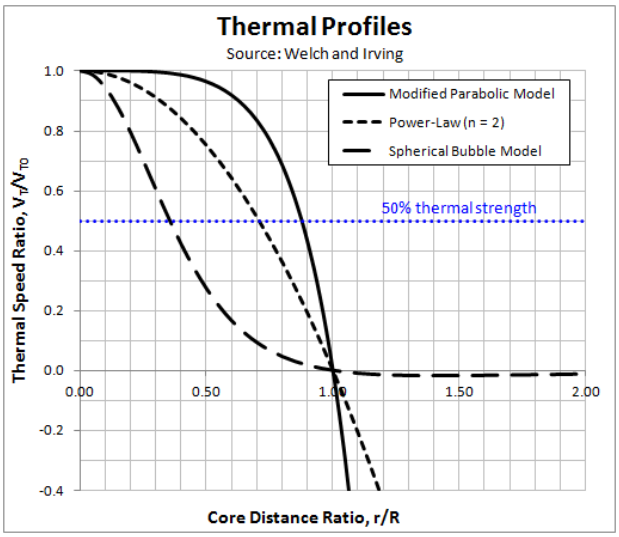

Figure C4-22: Common models used to approximate the vertical speed profile inside a thermal. r/R = 0

Reference 2 presents a number of thermal profiles, of which three are shown in Figure C4-22. Generally, the vertical speed in a thermal, denoted by V_T, will be greatest at its core. This maximum speed is denoted by V_{T0}. Even though the following mathematical models indicate the thermal is symmetrical, this is not necessarily so in real thermals. The three thermal profiles are defined mathematically below. The ratio r/R denotes the fractional distance from the center of a thermal whose diameter is 2R. Of the three presented, the Power-Law, using n = 2 is sometimes used for competition handicapping purposes[2], assuming a thermal radius of R = 1000 ft and with a core strength V_{T0} = 4.2 knots.

Power-Law Velocity Profile:
$$\frac{V_T}{V_{T0}} = 1-(r/R)^n \qquad \text{(C4-8)}$$

Spherical Bubble Model:
$$\frac{V_T}{V_{T0}} = \frac{1-(r/R)^2}{\left[1-2(r/R)^2\right]^{2.5}} \qquad \text{(C4-9)}$$

Modified Parabolic Model:
$$\frac{V_T}{V_{T0}} = \left[1-(r/R)^2\right]\cdot e^{-(r/R)^2} \qquad \text{(C4-10)}$$

The second element of thermal velocity profiles is their strength. Carmichael[10] defines thermal strength in as described below:

(1) *Strong thermal* has a maximum vertical speed of 20 ft/s (≈ 12 knots) that falls to 10 ft/s when r = 200 ft.
(2) *Weak thermal* has a maximum vertical speed of 10 ft/s (≈ 6 knots) that falls to 5 ft/s when r = 200 ft.
(3) *Wide thermal* has a maximum vertical speed of 15 ft/s (≈ 9 knots) that falls to 7.5 ft/s when r = 400 ft.

This information can be combined with the turn performance map to create a representation displaying the optimum bank angle given specific airspeed. This is shown for Sailplane A in Figure C4-23. The optimum climb for the selected airspeeds is easily identifiable. The map also shows that only airspeeds below 80 KCAS will result in climb in this condition and that exceeding 30° of bank is detrimental to the climb performance.

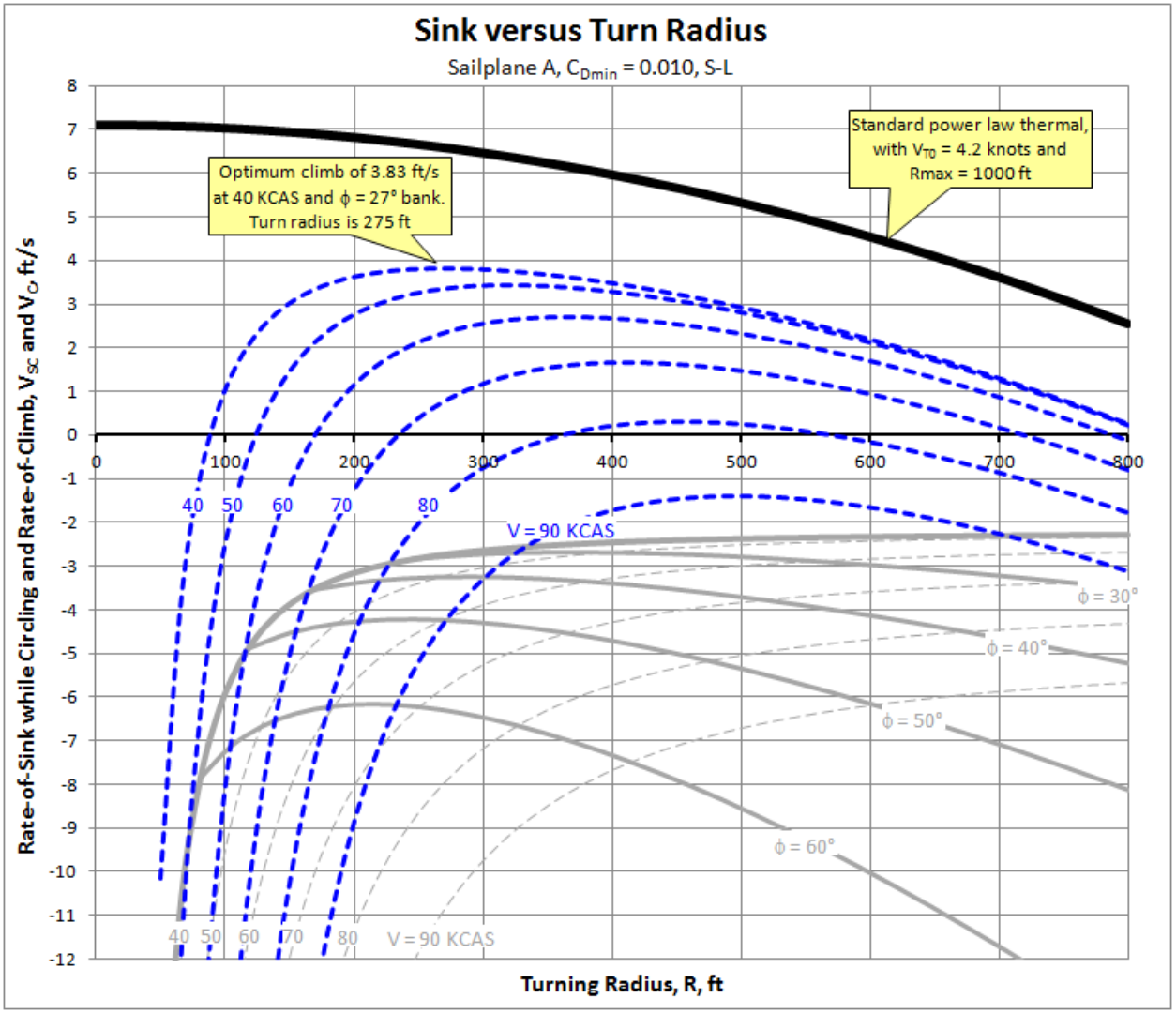

Figure C4-23: Turn performance map for Sailplane A assuming a maximum thermal radius of 1000 ft and core strength of 4.2 knots used to evaluate best ROC and the corresponding speed and bank angle.

The thick dashed, blue-colored curves in Figure C4-23 are obtained by adding V_T to the V_{SC}, which is calculated using Equation (C4-7). The value of V_T is calculated using any of the Equations (C4-8) through (C4-10). Effectively this shifts the fixed V_{SC} -isobars (the thin dashed gray-colored curves) upward into the new position, with the associated maximums.

C4.1.3 Constraint Diagram for a Sailplane

In addition to the preceding turn performance map, a constraint diagram can also be developed to learn more about design limitations. Constraint diagrams for powered aircraft are presented in Section 3.2, *Constraint Analysis*. The absence of power for sailplanes and gliders means that constraints other than T/W must be considered. The most obvious performance parameter is the Lift-to-Drag ratio (L/D). Just like the designer had to "presume" a likely minimum drag coefficient, C_{Dmin}, and Aspect Ratio, AR, this is also required for sailplanes. Then, for a given C_{Dmin} and AR, the question might be: Assuming the planform design will be such that an Oswald's efficiency of a given value, say 0.9, will be achieved, what wing loading, W/S, and LD_{max} yield desired airspeeds of the minimum sink, V_{BA}, or minimum angle (best glide), V_{BG}?

For instance, consider a scenario in which we are convinced our sailplane will achieve a C_{Dmin} = 0.008 and e = 0.95. It is of interest to determine the combinations of W/S and LD_{max} that renders V_{BA} = 45 KCAS and V_{BG} = 55 KCAS. This is what a sailplane constraint diagram can reveal. The development of such a diagram requires selected glide performance equations to be transformed into LD_{max} that is a function of W/S. Note that all the following expressions assume the simplified drag model. This is justified on the basis that the constraint diagram will get us a "ballpark" value.

LD_{max} for a Desired V_{BA}

The following expression is used to determine the combinations of W/S and LD_{max} required to achieve a desired airspeed of minimum sink rate at a given altitude. The airspeed must be true airspeed. The first step in its application is to convert the airspeed into dynamic pressure, q_{BA}. Then the constraint can be calculated using the following expression:

$$LD_{\max} = \frac{1}{\sqrt{C_{D\min}k + \left(\frac{k}{q_{BA}}\right)^2 \left(\frac{W}{S}\right)^2}} \tag{C4-11}$$

LD_{max} for a Desired V_{BG}

The following expression is used to determine the combinations of W/S and LD_{max} required to achieve a desired airspeed of minimum glide angle at a given altitude. The airspeed must be true airspeed. The first step in its application is to convert the airspeed into dynamic pressure, q_{BG}. Then the constraint can be calculated using the following expression:

$$LD_{\max} = \frac{1}{\sqrt{3C_{D\min}k + \left(\frac{k}{q_{BG}}\right)^2 \left(\frac{W}{S}\right)^2}} \tag{C4-12}$$

An example of the application of these formulas is shown in Figure C4-24. To read the graph, consider a sailplane slated to have an AR of 28 with an expected C_{Dmin} = 0.008 and e = 0.95, and for which a desired V_{BA} > 45 KCAS and V_{BG} > 55 KTAS. This is possible as long as its W/S is greater than 10.5 lbf/ft² and LD_{max} exceeds 48. For comparison, Reference 11 shows the Stemme S10 (for which this sample is intended to resemble) has a LD_{max} of 51, $V_{BA} \approx$ 45 KCAS, and $V_{BG} \approx$ 55 KCAS, at a W/S = 9.3 lb_f/ft^2, showing that this method is not far off the mark.

It should be stressed that a constraint diagram of this nature is not sufficient to design a sailplane. An optimization that takes into account it glide characteristics in thermals, as presented in the preceding section, is also called for.

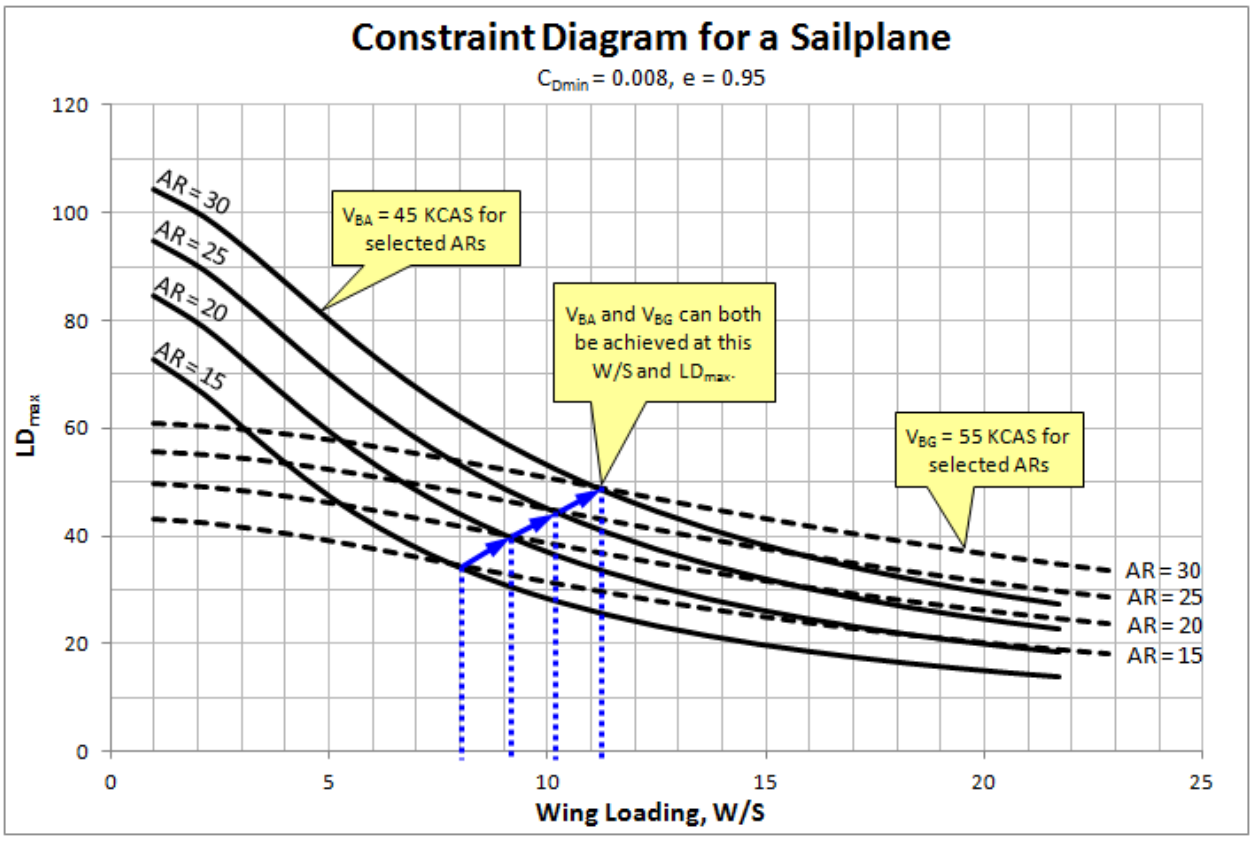

Figure C4-24: A constraint diagram for a hypothetical sailplane, whose C_{Dmin} and Oswald's efficiency factor are expected to be 0.010 and 0.9, respectively.

DERIVATION OF EQUATION (C4-11):

Begin with Equation (19-18) and rearrange as follows:

$$LD_{\max} = \frac{1}{\sqrt{4 \cdot C_{D\min} \cdot k}} \quad \Rightarrow \quad 4 \cdot C_{D\min} \cdot k = \frac{1}{LD_{\max}^2} \qquad \text{(i)}$$

Then, consider the expression for the airspeed of minimum sink rate, V_{BA}, given by Equation (21-14). Multiply the term under the second radical by k/k. Then, separate the altitude and W/S terms from the radical as follows:

$$V_{BA} = \sqrt{\frac{2}{\rho}\left(\frac{W}{S}\right)\sqrt{\frac{k}{3C_{D\min}}}} = \sqrt{\frac{2}{\rho}\left(\frac{W}{S}\right)\sqrt{\frac{k^2}{3C_{D\min}k}}} = \sqrt{\frac{2}{\rho}\left(\frac{W}{S}\right)}\left(\frac{k^2}{3C_{D\min}k}\right)^{1/4}$$

Then, add and subtract C_{Dmin}·k from the denominator of the quartic:

$$V_{BA} = \sqrt{\frac{2}{\rho}\left(\frac{W}{S}\right)}\left(\frac{k^2}{3C_{D\min}k}\right)^{1/4} = \sqrt{\frac{2}{\rho}\left(\frac{W}{S}\right)}\left(\frac{k^2}{4C_{D\min}k - C_{D\min}k}\right)^{1/4}$$

The positive term in the denominator of the quartic is the square of the LD_{max}. Insert to get:

$$V_{BA} = \sqrt{\frac{2}{\rho}\left(\frac{W}{S}\right)}\left(\frac{k^2}{1/LD_{\max}^2 - C_{D\min}k}\right)^{1/4}$$

Square both sides and note that $q_{BG} = \frac{1}{2}\rho V_{BG}^2$

$$V_{BA}^2 = \frac{2}{\rho}\left(\frac{W}{S}\right)\sqrt{\frac{k^2}{1/LD_{\max}^2 - C_{D\min}k}} \quad \Leftrightarrow \quad \left(\frac{q_{BA}}{(W/S)}\right)^2 = \frac{k^2}{1/LD_{\max}^2 - C_{D\min}k}$$

Then, solve for LD_{max}:

$$1/LD_{\max}^2 - C_{D\min}k = \frac{k^2\left(\frac{W}{S}\right)^2}{q_{BA}^2} = \left(\frac{k}{q_{BA}}\right)^2\left(\frac{W}{S}\right)^2 \quad \Leftrightarrow \quad LD_{\max} = \sqrt{\frac{1}{C_{D\min}k + \left(\frac{k}{q_{BA}}\right)^2\left(\frac{W}{S}\right)^2}}$$

QED

DERIVATION OF EQUATION (C4-11):

Proceed in a similar fashion as above using the expression for the airspeed of minimum glide angle, V_{BG}, given by Equation (21-16). Multiply the term under the second radical by k/k. Then, separate the altitude and W/S terms from the radical as follows:

$$V_{BG} = \sqrt{\frac{2}{\rho}\left(\frac{W}{S}\right)\sqrt{\frac{k}{C_{D\min}}}} = \sqrt{\frac{2}{\rho}\left(\frac{W}{S}\right)\sqrt{\frac{k^2}{C_{D\min}k}}} = \sqrt{\frac{2}{\rho}\left(\frac{W}{S}\right)}\left(\frac{k^2}{C_{D\min}k}\right)^{1/4}$$

Then, add and subtract $3C_{Dmin}$·k from the denominator of the quartic:

$$V_{BA} = \sqrt{\frac{2}{\rho}\left(\frac{W}{S}\right)}\left(\frac{k^2}{C_{D\min}k + 3C_{D\min}k - 3C_{D\min}k}\right)^{1/4} = \sqrt{\frac{2}{\rho}\left(\frac{W}{S}\right)}\left(\frac{k^2}{4C_{D\min}k - 3C_{D\min}k}\right)^{1/4}$$

The positive term in the denominator of the quartic is the square of the LD_{max}. Insert to get:

$$V_{BA} = \sqrt{\frac{2}{\rho}\left(\frac{W}{S}\right)}\left(\frac{k^2}{1/LD_{\max}^2 - 3C_{D\min}k}\right)^{1/4}$$

Square both sides and note that $q_{BA} = \frac{1}{2}\rho V_{BA}^2$

$$V_{BA}^2 = \frac{2}{\rho}\left(\frac{W}{S}\right)\sqrt{\frac{k^2}{1/LD_{\max}^2 - 3C_{D\min}k}} \quad \Leftrightarrow \quad \left(\frac{q_{BA}}{(W/S)}\right)^2 = \frac{k^2}{1/LD_{\max}^2 - 3C_{D\min}k}$$

Then, solve for LD_{max}:

$$1/LD_{\max}^2 - 3C_{D\min}k = \frac{k^2\left(\frac{W}{S}\right)^2}{q_{BA}^2} = \left(\frac{k}{q_{BA}}\right)^2\left(\frac{W}{S}\right)^2 \quad \Leftrightarrow \quad LD_{\max} = \sqrt{\frac{1}{3C_{D\min}k + \left(\frac{k}{q_{BA}}\right)^2\left(\frac{W}{S}\right)^2}}$$

QED

C4.1.4 Sailplane Tail Design

Designing the empennage for a sailplane is identical to that of powered airplanes, minus the thrust contribution, unless of course, the sailplane is powered. The tail should be sized such that handling and controllability complies with the applicable paragraphs of CS-22 (EASA Certification Specifications for Sailplanes and Powered Sailplanes). In particular, this involves Subpart B, Flight, paragraphs 22.21 through 22.255.

Just like the conceptual design of powered aircraft, the first estimation can be made using the conventional historical tail volume methods of Section 11.5, *Initial Tail Sizing Methods*. This will get the tail size in the "ballpark." The next step is to evaluate if the resulting geometry provides the necessary elevator or rudder authority during some extreme conditions stipulated in Subpart B. For a sailplane, cross-wind landing, stalling and flaps down at low airspeeds with a forward CG position, and possibly aerotow or winch operations during T-O would present a challenge. There is no balked landing case to contend with, unless the sailplane is powered.

Requirements for Elevator Deflection to Trim

Equation (11-25) can be used to estimate the AOA and elevator deflection to trim at various conditions. The expression is presented in its simplified form below, by setting all thrust terms to 0:

$$\begin{bmatrix} C_{D_\alpha} & C_{D_{\delta_e}} \\ C_{L_\alpha} & C_{L_{\delta_e}} \\ C_{m_\alpha} & C_{m_{\delta_e}} \end{bmatrix} \begin{Bmatrix} \alpha \\ \delta_e \end{Bmatrix} = \begin{Bmatrix} -C_{D_{\min}} - C_{D_{\delta_f}}\delta_f \\ \frac{W}{qS} - C_{L_0} - C_{L_{\delta_f}}\delta_f \\ -C_{m_0} - C_{m_{\delta_f}}\delta_f \end{Bmatrix} \tag{C4-13}$$

The terms are detailed in Chapter 11, *The Anatomy of the Tail*. The formulation allows the effect of flaps as means to lower stalling speed or as cruise flaps to be included. The expression should be used to estimate if excessive elevator deflection is required for the maneuvers stipulated in CS-22. If so, the elevator and the HT geometry must be resized.

Stick-Fixed Neutral Point

Equation (11-26), reproduced below for convenience, can be used to estimate the location of the stick fixed neutral point:

$$\frac{h_n}{C_{MGC}} = \frac{h_{AC}}{C_{MGC}} + V_{HT} \cdot \frac{C_{L_{\alpha_{HT}}}}{C_{L_\alpha}} \cdot \left(1 - \frac{2C_{L_\alpha}}{\pi \cdot AR}\right) - \frac{C_{m_{\alpha_{AC}}}}{C_{L_\alpha}} \tag{11-26}$$

Again, see Chapter 11 for the definition of terms. Note that it is assumed that the tail efficiency for a sailplane is $\eta_{HT} \approx 1$, so it is omitted from the equation. Since the horizontal tail volume is defined as $V_{HT} = \frac{S_{HT} \cdot l_{HT}}{S \cdot C_{MGC}}$, the expression can be used to estimate the product $S_{HT} \cdot l_{HT}$ for a given wing geometry and expected (or desired) Static Margin (SM), defined as follows:

$$SM = (h_n - h)/C_{MGC} \tag{C4-14}$$

Where h and h_n are the physical location of the CG and stick-fixed neutral point measured from the LE of the C_{MGC}. Note that a 10% SM would be represented as 0.1 and so on. Introducing this to Equation (11-26) and assuming a typical value of $h_{AC}/C_{MGC} \approx 0.25$ leads to:

$$SM = \frac{(h_n - h)}{C_{MGC}} = 0.25 - \frac{h}{C_{MGC}} + V_{HT} \cdot \frac{C_{L_{\alpha HT}}}{C_{L_\alpha}} \cdot \left(1 - \frac{2C_{L_\alpha}}{\pi \cdot AR}\right) - \frac{C_{m_{\alpha AC}}}{C_{L_\alpha}} \tag{11-15}$$

This can be solved for the required horizontal tail volume as shown below:

$$V_{HT} = \left(SM - 0.25 + \frac{h}{C_{MGC}} + \frac{C_{m_{\alpha AC}}}{C_{L_\alpha}}\right) \frac{C_{L_\alpha}}{C_{L_{\alpha HT}}} \frac{\pi \cdot AR}{(\pi \cdot AR - 2C_{L_\alpha})} \tag{11-16}$$

Once a suitable V_{HT} has been determined, it is possible to optimize the tail arm length with respect to drag by minimizing the wetted area. Such an optimization is identical to Methods 1 through 3 of Section 11.5, except that the contraction of complex geometry may call for a numerical scheme to be implemented, rather than a closed form analytical solution. In order to demonstrate how such optimization can be accomplished, a simplified approximation of the tadpole configuration is represented below using two frustums.

Initial Tail Sizing Optimization using an Arbitrary Fuselage

Figure 12-3 shows a textbook tadpole fuselage from the side. While the contraction of the fuselage for real applications is carefully crafted, a simplification like the one shown in Figure 12-25 can be utilized to demonstrate the determination a tail arm length for a tadpole fuselage. The approach minimizes the combined wetted area of the HT, VT, and tailboom, thus, minimizing skin friction drag. For convenience, the figure is reproduced below as Figure C4-25, with the addition of a wing and HT, to better clarify the assumptions to be made. It must be stressed that this method is only a geometric optimization. It does not guarantee that flow separation will not happen. If the contraction of the aft fuselage is too rapid, the flow will separate, increasing the drag. The final shape will have to be refined using a more sophisticated CFD analysis or wind tunnel testing to confirm that flow separation does not occur.

For this optimization, it will be assumed that the forward part of the fuselage is only shaped to sustain NLF as far back as possible. Typically, the NLF transitions into turbulent boundary layer near the LE of the wing. For this reason, the forward part of the fuselage is assumed to not influence the required tail arm length. Therefore, it is simply omitted from further consideration. The part of the fuselage of importance in the development of this method extends approximately from the wing's quarter chord to that of the HT, as shown in Figure C4-25. This leaves us with the following control variables: L_3, L_4, D, d_1, and d_2. Furthermore, it will take into account a desired V_{HT} and V_{VT}, identical to the approach of Section 11.5.3, *METHOD 3: Initial Tail Sizing Optimization Considering Horizontal and Vertical Tail*.

Using these variables, the following formulas can be used to estimate the wetted area of the tail boom, but these are taken directly from the approach of Section 12.4.4, *Surface Areas and Volumes of a Tadpole Fuselage* by using Equation (12-10). Note that for convenience, the diameter variables will be related to the maximum fuselage diameter, D, as follows:

$$d_1 = rD \quad and \quad d_2 = sD$$

Additionally, let's define the constant k: $k = L_3/l_T$

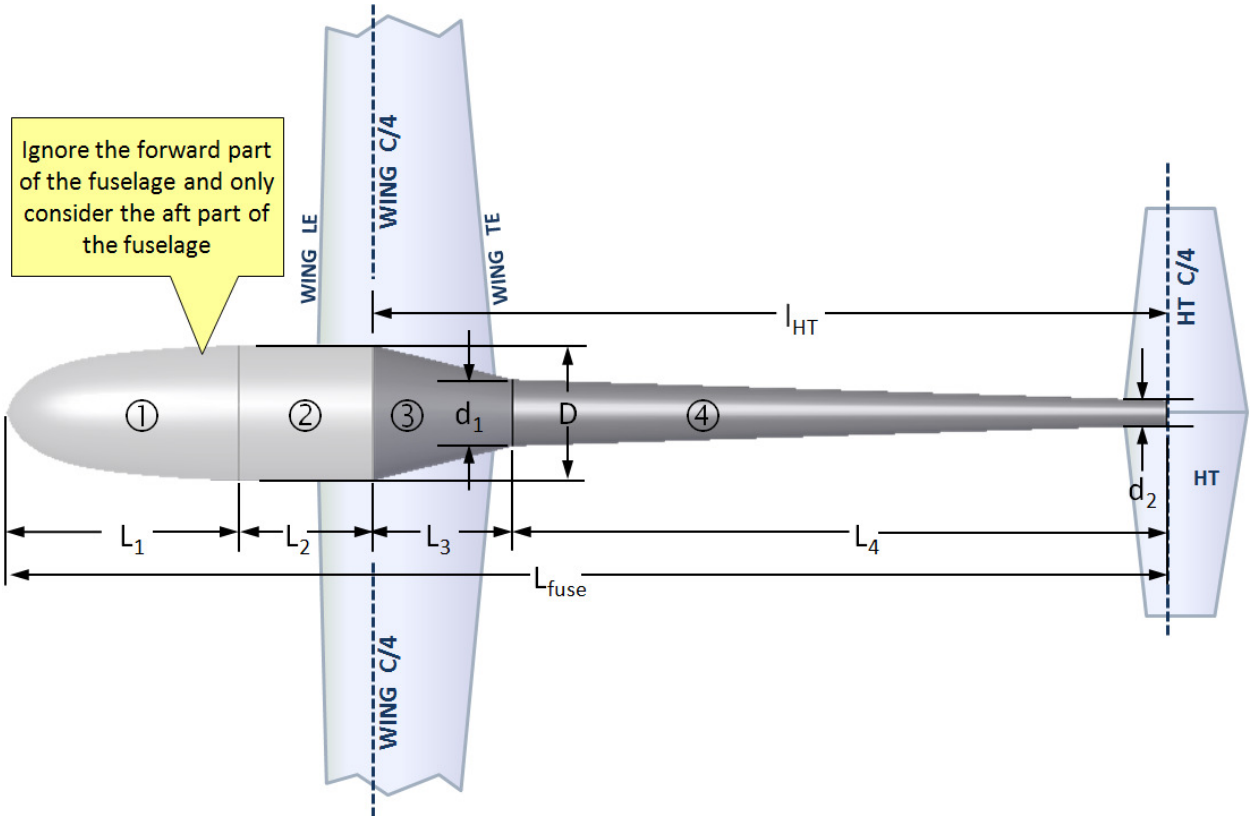

Figure C4-25: An approximation of a tadpole fuselage using elementary solids. Only the section of the fuselage between quarter chord of the wing and HT are considered.

This reduces the number of variables from five to two. We can now write:

Tail arm length:
$$l_{HT} = L_3 + L_4 \quad \Rightarrow \quad L_3 = k l_{HT} \quad and \quad L_4 = (1-k) l_{HT} \tag{C4-17}$$

Wetted area of frustum ③:
$$S_{F1} = \frac{\pi D(1+r)}{2}\sqrt{k^2 l_{HT}^2 + \frac{D^2}{4}(1-r^2)} \tag{C4-18}$$

Wetted area of frustum ④:
$$S_{F2} = \frac{\pi D(r+s)}{2}\sqrt{(1-k)^2 l_{HT}^2 + \frac{D^2}{4}(r^2-s^2)} \tag{C4-19}$$

The total wetted area of the aft fuselage is the sum of S_{F1} and S_{F2}:

$$S_F = \frac{\pi D}{2}\left((1+r)\sqrt{k^2 l_{HT}^2 + \frac{D^2}{4}(1-r^2)} + (r+s)\sqrt{(1-k)^2 l_{HT}^2 + \frac{D^2}{4}(r^2-s^2)}\right) \tag{C4-20}$$

Also, it is of interest to compare the wetted area of the tadpole fuselage to that of a standard frustum shape, S_{Fstd}. This is easily calculated using Equation (12-10), where $D_1 = D$ and $D_2 = d_2 = sD$ in Figure C4-25. The resulting expression is given by:

Standard frustum:

$$S_{Fstd} = \left(\frac{\pi D(1+s)}{2} \sqrt{l_{HT}^2 + \frac{D^2}{4}\left(1 - s^2\right)} \right) \qquad \text{(C4-21)}$$

Numerical comparison using typical sailplane geometry reveals that the reduction in surface area of a tadpole is easily in the 20-35% range. All of the above equations are simple to derive using Equation (12-10). Additional equations required are Equations (11-57) and (11-58), which are needed to calculate the planform areas of the HT and VT, from which an approximation to their corresponding wetted areas is generated. In other words, if V_{HT} and V_{VT} have been established, it is possible to calculate a corresponding S_{HT} and S_{VT}, which are then converted into wetted areas. In its simplest form, the wetted area for the HT is $2 \cdot S_{HT}$, although multiplying this by a factor like 1.05 to account for airfoil curvature is a more reasonable approach. An example of their use for a geometric optimization is given below.

EXAMPLE C4-2:
Consider the Stemme S-10 style geometry shown in Figure C4-26. Note that the dimensions given may not necessarily match that of the Stemme, as the purpose here is only to see if the above optimization will yield a similar tail arm. Judging from three-views of the aircraft that are in the public domain, its tail arm (l_T) is about 16.7 ft. The wing area is 201.3 ft², wing span is 75.5 ft, AR is 28.3, and a representative Taper Ratio of about 0.3 is assumed. This results in a C_{MGC} of 2.924 ft. Further assume the fuselage can be approximated using the tadpole diagram of Figure C4-25, has a contraction location of $0.25 \cdot l_T$, a max diameter of 3.75 ft, r = 0.4, and s = 0.156. Determine the tail arm length, l_T, that yields the minimum combined wetted area of the HT, VT, and tailboom using historical values of V_{HT} = 0.5 and V_{VT} = 0.2, from Table 11-4. Use a 1.05 wetted area booster for the HT and VT.

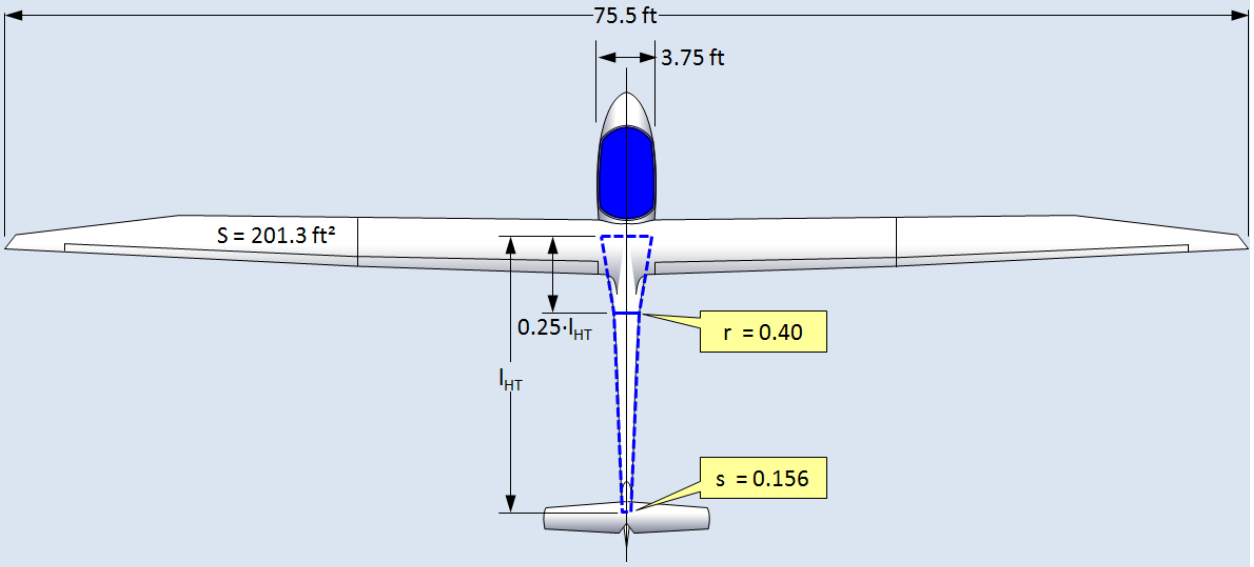

Figure C4-26: A Stemme S-10 style geometry.

SOLUTION:
The solution is best accomplished by calculating the wetted area for a number of possible tail arm lengths, ideally using a spreadsheet. This has been done in the Table C4-3 below. In the table, l_{HT} varies from 5 to 20 ft. The columns containing S_{HT} and S_{VT} were calculated using Equations (11-57) and (11-58) with the cited tail volumes. The wetted areas in the next two columns is calculated using $S_{HT\ WET} = 2 \cdot S_{HT} \cdot 1.05$ and $S_{VT\ WET} = 2 \cdot S_{VT} \cdot 1.05$, respectively. The columns containing S_{F1} and S_{F2} were calculated using Equations (C4-18) and (C4-19). The column labeled S_{WET} is the total wetted area (the cost function). It is simply the sum $S_{HT\ WET} + S_{VT\ WET} + S_{F1} + S_{F2}$. Finally, the column labeled S_{Fstd} was calculated using Equation (C4-21) and the last column is the ratio of wetted areas of the standard frustum to the tadpole tailboom. For instance, if l_T = 20 ft, the wetted area of the standard frustum is 27.8% greater than that of the tadpole.

A very pronounced minimum can be seen in the accompanying graph. It was found to correspond to an l_T of 16.0 ft, although a more accurate evaluation shows it is closer to 15.8 ft. However, a tail boom length ranging from 14 to 18 ft will result in near optimum wetted area, giving the designer some flexibility when sizing the tail. Both values are not too far from the reference value of 16.7 ft of the actual Stemme S-10. Note that analysis of a three-view of the sailplane shows it has a $V_{HT} \approx 0.44$ and $V_{VT} \approx 0.018$. Similarly, its $S_{HT} \approx 15.5$ ft² and $S_{VT} \approx 15.1$ ft².

Table C4-3: Results from Tail Arm Optimization

l_{HT}	S_{HT}	S_{VT}	$S_{HT\ WET}$	$S_{VT\ WET}$	S_{F1}	S_{F2}	S_{WET}	S_{Fstd}	$S_{Fstd}/(S_{F1}+S_{F2})$
5.0	58.86	60.79	123.60	127.66	17.52	16.00	284.79	36.29	1.083
6.0	49.05	50.66	103.00	106.39	18.81	19.15	247.35	42.74	1.126
7.0	42.04	43.42	88.29	91.19	20.23	22.30	222.00	49.29	1.159
8.0	36.79	38.00	77.25	79.79	21.75	25.45	204.24	55.89	1.184
9.0	32.70	33.77	68.67	70.92	23.35	28.61	191.55	62.54	1.204
10.0	29.43	30.40	61.80	63.83	25.02	31.77	182.42	69.23	1.219
11.0	26.75	27.63	56.18	58.03	26.74	34.93	175.88	75.93	1.231
12.0	24.52	25.33	51.50	53.19	28.51	38.09	171.30	82.65	1.241
13.0	22.64	23.38	47.54	49.10	30.32	41.25	168.21	89.38	1.249
14.0	21.02	21.71	44.14	45.59	32.15	44.42	166.31	96.13	1.255
15.0	19.62	20.26	41.20	42.55	34.02	47.58	165.36	102.88	1.261
16.0	18.39	19.00	38.63	39.90	35.90	50.75	165.17	109.64	1.265
17.0	17.31	17.88	36.35	37.55	37.81	53.91	165.62	116.40	1.269
18.0	16.35	16.89	34.33	35.46	39.72	57.08	166.60	123.17	1.272
19.0	15.49	16.00	32.53	33.60	41.66	60.25	168.02	129.94	1.275
20.0	14.71	15.20	30.90	31.92	43.60	63.41	169.83	136.72	1.278

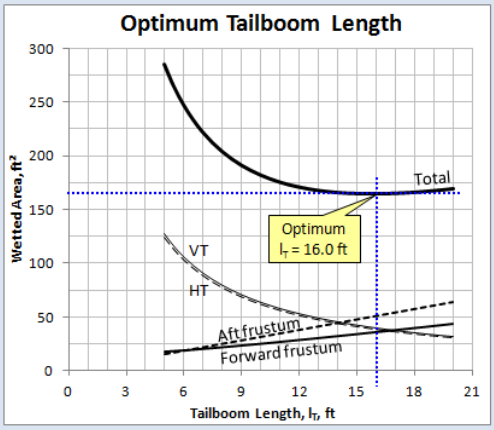

C4.1.5 Sailplane Design Tips

With the exception of the importance of glide performance, the design of sailplanes is not all that different from powered airplanes. Requirements for structures (weight, strength, stiffness), fabrication (manufacturing cost, maintenance cost, material selection, production methodologies), ergonomics (field-of-view, control system methodologies, cockpit accommodation), and flying qualities (natural static and dynamic stability, stall characteristics) are similar in many ways. Certification requirements have many similarities and differences. Ground handling of sailplanes is different as many allow for quick assembly and disassembly. Also, take-off using aero-tow or winches must be considered. The same holds for jettisonable water ballast, generally not used in powered GA aircraft. The high glide ratio of sailplanes calls for speed brakes or spoilers to allow for a steeper approach path on final.

The certification of sailplanes and powered sailplanes is generally done through EASA standard CS-22, *EASA Certification Specifications for Sailplanes and Powered Sailplanes*. As stated in Table 1-1, 14 CFR 21.17(b) allows the FAA to tailor the certification on a need-to-basis to sailplanes. Then, by referring to AC 21.17-2A, the FAA accepts the former JAR-22 (now CS-22) as a certification basis.

In addition to the preceding discussion, the following tips should be considered by the designer of sailplanes.

1	To improve climb performance	• Reduce wing loading for improved circling characteristics • Increase AR • Increase Reynolds number • Reduce C_{Dmin} and C_{Dmisc} • Use a wing planform that best achieves elliptical lift distribution • Consider the use of winglets or polyhedral planform
2	Cross-country performance	• Increase wing loading for higher interthermal airspeeds • Increase AR • Increase Reynolds number • Reduce C_{Dmin} and C_{Dmisc} • Use a wing planform that best achieves elliptical lift distribution • Consider the use of winglets or polyhedral planform

3	Surface qualities	• The surface quality of sailplanes must be very smooth to stabilize the NLF. • Composites are currently the best material for high-quality sailplane construction • Class A surface qualities, which means that surface curvature, slope and alignment of surfaces should be continuous wherever possible.
4	Wing design	• Consider wing planform shapes that generate constant section lift coefficients along the span (elliptical lift distribution) • High aspect ratio, as long as its structural weight impact is light • Consider cruise flaps • Seal gaps not needed for aerodynamic purposes. A gap between aileron and wing is generally detrimental. A gap between a slotted flap and wing is beneficial • NLF airfoils
5	Fuselage design	• Tadpole fuselage geometry • Smooth surface qualities with faired intersections between it and the lifting surfaces • Retractable landing gear • One piece canopy with smooth

C4.1.6 Design of Unmanned Aerial Vehicles

Just like the design of sailplanes, the design of *Unmanned Aerial Vehicles* (UAV) is far more involved than appears at first glance. This is primarily due to the use of an autopilot that often must be capable of autonomous take-off and landing. What aerodynamic appearance concerns, the UAV can be designed just like any other airplane. However, the absence of human operators often calls for geometry dictated more by utility than aerodynamics and, often, this results in statically unstable aircraft.

Configuration B in Figure C4-2 is one practical solution of many for a simple powered airplane with good long-range or long-endurance reconnaissance mission, designed by the author for a UAV project. It features a tailboom intended to protect the propeller as it was expected to land on unimproved strips. The T-tail was selected to ensure it resides in the propwash to improve responsiveness at the low airspeeds, which is where the vehicle was designed to operate most of the time. It also protects the tail when landing, as it ensures the plane will come to rest on its wing. The cranked wing planform features a straight leading edge, but forward swept quarter chord naturally diminishes section lift coefficients at the tip to improve roll stability a stall. This is compounded by the cranked dihedral and, thus, reduces the need for excessive washout. It also helps to protect the wingtip if the airplane lands on unimproved strips with ground vegetation. The size of the HT depends on the high thrust line, which is necessitated by adequate propeller clearance.

UAVs have become very practical for tasks that for the most part require monotonous flying. The advent of small but sophisticated autopilots and electronic gyros is in the process of transforming this branch of aviation. Such aircraft are primarily intended for surveillance and research flight. They are often equipped with cameras that are capable of tracking landmarks and transmit a live signal that also allows them to be flown manually from great distances. Generally, the airframe is regarded as a platform to carry electronic surveillance equipment. For this reason, many UAVs do not take advantage of advanced aerodynamics and it can be argued that selecting a tried configuration is beneficial to some unusual configurations. Therefore, any of the aforementioned configurations will work and many of the arguments for or against are applicable to the UAVs and the one's that involve the human factor can be ignored.

REFERENCES

[1] NASA CR-2315, *Motorless Flight Research*, Althaus, Dieter, 1972.
[2] Welch, Ann, Lorne Welch, and Frank Irving, *The Complete Soaring Pilot's Handbook*, David McKay Company, 1977.
[3] Fédération Aéronautique Internationale, Record ID 14043. Website is www.fai.org.
[4] Fédération Aéronautique Internationale, Record ID 8198.
[5] Boermans, L. M. M., *Research on sailplane aerodynamics at Delft University of Technology - Recent and Present Developments*, presented to Netherlands Association of Aeronautical Engineers (NVvL), 2006.
[6] Thomas, Fred, *Fundamentals of Sailplane Design*, College Park Press, 1999.
[7] Reichmann, Helmut, *Cross-Country Soaring*, 2nd Ed., Soaring Society of America, 1993.
[8] Stewart, Ken, *The Soaring Pilot's Manual*, 2nd Ed., Airlife Publishing, 2008.
[9] Scull, Bill, *Soaring Across Country*, Pelham Books, 1979.
[10] Carmichael, Bruce H., *What Price Performance*, Soaring Magazine, May-June, 1954.
[11] Anonymous, *Flight Manual Stemme S10-V*, Stemme AG, 1994.